Available online at www.sciencedirect.com

ScienceDirect

Geochimica et Cosmochimica Acta 314 (2021) 121–139

Geochimica et Cosmochimica Acta

www.elsevier.com/locate/gca

Reversible scavenging and advection – Resolving the neodymium paradox in the South Atlantic

Ruixue Wang [a,*], Josephine A. Clegg [a], Peter M. Scott [b,1], Christina S. Larkin [a,c], Feifei Deng [b,2], Alexander L. Thomas [b,3], Xin-Yuan Zheng [b,4], Alexander M. Piotrowski [a]

[a] Department of Earth Sciences, University of Cambridge, UK
[b] Department of Earth Sciences, University of Oxford, UK
[c] School of Ocean and Earth Science, National Oceanography Centre, University of Southampton, UK

Received 31 January 2021; accepted in revised form 12 September 2021; available online 20 September 2021

Abstract

Significant gaps in our understanding of the oceanic cycling of neodymium (Nd) and the other rare earth elements (REEs) remain despite decades of research. One important observation which has not been adequately explained is that the concentration of dissolved Nd typically increases with depth, similar to nutrient profiles, while Nd isotopes appear to reflect conservative water mass mixing in the intermediate and deep ocean; this has been termed the "Nd paradox". Here we present a detailed study of the dissolved Nd isotopic composition across a section at 40°S in the South Atlantic, collected by UK GEOTRACES cruise (section GA10). The South Atlantic represents a natural laboratory for our understanding of spatial controls on ocean geochemistry, because of the large variability of inputs, spatial differences in particulate cycling, and horizontal advection and mixing at depth between major northern- and southern-sourced water masses. This variability has also made the South Atlantic a critical region subject to intense investigations that aim at reconstructing past changes in ocean processes, such as changes in biological productivity and deep ocean circulation.

Our Nd isotope results from the GA10 section provide observational data show the signal of water mass mixing and reversible scavenging. In the surface ocean (0–600 m), Nd isotopic compositions are distinct between different surface ocean currents and spatially can be tied to various continental sources. In the intermediate ocean (600–2500 m), the vertical Nd isotope distribution exhibits distinct signals of different water masses by horizontal advection, including upper North Atlantic Deep Water and Antarctic Intermediate Water formed in the Atlantic Ocean or the Indian Ocean. The Nd isotope distribution also reflects influence of reversible scavenging that smears the signals downwards in the water column (i.e., offset to more radiogenic values). In the deep ocean below 2500 m, Nd isotope distribution largely follows conservative water mass mixing model. Nd concentration in the deep ocean, however, deviates from conservative mixing and increases constantly with depth. We also observe that Nd isotopes appear to be shifted towards the composition of overlying water masses. These observations suggest that reversible scavenging of Nd onto organic and other types of particles is a major vertical process throughout the water column. We also suggest that this process can resolve the "Nd paradox" of decoupling of Nd concentration and isotopic composition due to mixing dynamics. Because abyssal water masses already have a high Nd concentration, a given amount of Nd

* Corresponding author.
E-mail address: rw581@cam.ac.uk (R. Wang).
[1] Now at: Centre for Microscopy, Characterisation & Analysis, The University of Western Australia, Australia.
[2] Now at: Helmholtz-Zentrum Geesthacht, Germany.
[3] Now at: School of GeoSciences, University of Edinburgh, UK.
[4] Now at: Department of Earth and Environmental Sciences, University of Minnesota-Twin Cities, USA.

https://doi.org/10.1016/j.gca.2021.09.015

added from the vertical process has less of an effect on Nd isotopic compositions in deep water masses than it does for intermediate water masses which have comparatively low Nd concentration.

Keywords: Neodymium isotopes; Neodymium cycling; Nd paradox; South Atlantic; GEOTRACES

1. INTRODUCTION

Neodymium (Nd) is one of the rare earth elements (REEs) and its isotopic composition (usually expressed as $\varepsilon_{Nd} = [(^{143}Nd/^{144}Nd)_{sample}/(^{143}Nd/^{144}Nd)_{CHUR} - 1] * 10000$ with CHUR as Chondritic Uniform Reservoir) has been widely used as a proxy for both present and past ocean circulation. This is because the residence time of Nd in the ocean has been estimated to be 10^2–10^3 years (Tachikawa et al., 1999; Siddall et al., 2008; Rempfer et al., 2011), long enough to be transported within the global thermohaline circulation system but short enough to avoid complete homogenization. Neodymium is delivered to the ocean, together with other REEs, by continental weathering via dissolved and particulate loads of rivers and aeolian dust (Goldstein et al., 1984; Frank, 2002; Goldstein and Hemming, 2003) as well as through exchange with continental margins (Lacan and Jeandel, 2005; Jeandel, 2016). Once input to the ocean, Nd can be adsorbed on particle surfaces due to the particle-reactive attribute of REEs. Because of higher reactivity of light REEs (LREEs: Lanthanum to Samarium) relative to heavy ones (HREEs: Europium to Lutetium), shale-normalized (Post Archean Australian Shale or PAAS; Taylor and McLennan, 1985) REE patterns in open-ocean seawater typically display a tilted shape with an enrichment in HREEs relative to LREEs (Elderfield et al., 1988; Byrne and Kim, 1990; Zheng et al., 2016).

Dissolved Nd concentrations ([Nd]) in major ocean basins away from the continent are relatively depleted in surface waters while enriched in deep waters. There is an overall nutrient-like increase in dissolved [Nd] from the deep North Atlantic to the deep North Pacific. However, seawater ε_{Nd} in the intermediate and deep ocean broadly reflects conservative mixing between water mass endmember compositions (Tachikawa et al., 2017). Water mass endmembers in the Atlantic Ocean typically have less radiogenic ε_{Nd} values, such as ~ -13 in the North Atlantic Deep Water (NADW) (Goldstein and Hemming, 2003; Lambelet et al., 2016), whereas North Pacific waters often have more radiogenic values between -2 and -4 (Piepgras and Jacobsen, 1988; Amakawa et al., 2009; Fuhr et al., 2021) due to varied continental sources with different Nd isotopic ratios. Those two most significant end members mix within the Antarctic Circumpolar Current (ACC), resulting in an intermediate ε_{Nd} value of ~ -8.5 (Piepgras and Wasserburg, 1982; Stichel et al., 2012).

The decoupling of Nd concentrations and isotopic compositions in the ocean has been termed the "Nd paradox" (e.g., Goldstein and Hemming, 2003). Previous studies have tried to explain the "Nd paradox" by reversible particle scavenging (Siddall et al., 2008; Molina-Kescher et al., 2014; Stichel et al., 2015), particularly in high productivity areas (e.g., Grasse et al., 2012) or near large river mouths (Singh et al., 2012). Reversible scavenging refers to the process during which an element is in dynamic equilibrium between sorption and desorption with particle surfaces throughout the water column, resulting in scavenge onto particles and later release into the deeper water masses. The desorption can be caused by particle dissolution, aggregation/disaggregation, or variation in the dissolved concentration of the element as particles sink down through the water column. Another alternative explanation for higher [Nd] at depth is a widespread benthic diffusive flux of Nd from the bottom of the ocean basins perhaps due to sediment or sediment-phase dissolution (Haley et al., 2004; Abbott et al., 2015). However, direct measurements of benthic flux are largely restricted to marginal settings to date, and an unambiguous test for the global extent of this flux remains to be established.

Recently, with the effort of the international GEOTRACES program, a growing dataset of modern dissolved (van de Flierdt et al., 2016; Amakawa et al., 2019; Zieringer et al., 2019; Rahlf et al., 2020) and suspended particulate matter (SPM; Lagarde et al., 2020; Stichel et al., 2020) Nd concentrations and isotopic compositions in different ocean basins has been established as well as the implementation of extensive modelling studies (Siddall et al., 2008; Rempfer et al., 2011; Oka et al., 2021). Here we present a detailed study of distribution of dissolved ε_{Nd} along the 40°S South Atlantic section (GA10). The South Atlantic is a key area for paleoceanographic studies because at depth it is a good location to monitor changes of the global deep ocean circulation (e.g. North Atlantic Deep Water and Antarctic Bottom Water) through time (e.g., Piotrowski et al., 2005), and carbon storage of the ocean over glacial to inter-glacial time scales (e.g. Farmer et al., 2019). Relevant to Nd cycling, this region features large variations in biological productivity due to strong gradients in surface ocean nutrient concentrations (Sarmiento et al., 2004). Here, we examine vertical cycling processes in areas of high productivity and oligotrophic conditions, and with differing particle fluxes, at different depths and distances from boundaries in order to put quantitative constraints on Nd concentration and isotopic composition change and therefore explain the "Nd paradox".

1.1. Hydrography

The major ocean currents in the South Atlantic at different depths are shown in Fig. 1. We present the hydrography of section GA10 along 40°S based on the distribution of temperature (θ) and salinity (S) (Fig. 2a, 2b), following Wyatt et al. (2014). In the surface ocean, warm and salty

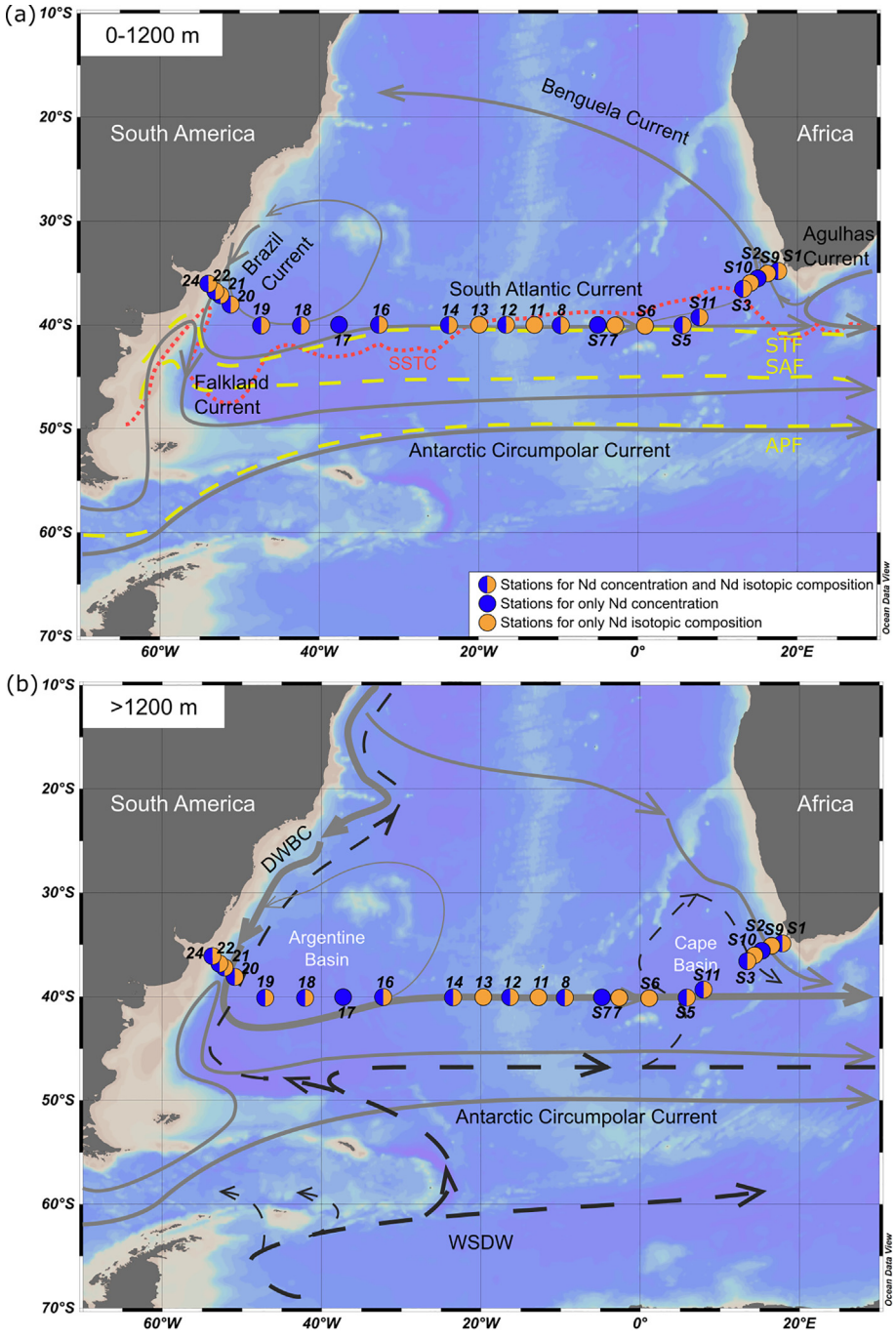

Fig. 1. Map of GA10 stations with (a) surface currents (0–1200 m) and (b) intermediate and deep currents (>1200 m). Currents are simplified following Stramma and England (1999). STF: Sub-Tropical Front; SAF: Sub-Antarctic Front; APF: Antarctic Polar Front; DWBC: Deep Western Boundary Current; WSDW: Weddell Sea Deep Water; SSTC: South Subtropical Convergence.

Sub-Tropical Surface Water (STSW, $\theta > 15$ °C, $S > 35.2$) meets the cold and fresh Sub-Antarctic Surface Water (SASW, $\theta < 15$ °C, $S < 34.8$) in the open sea at 40°S. The South Subtropical Convergence (SSTC) crosses 40°S in the South Atlantic Ocean, an intersection point of low macronutrient subtropical gyre waters meet high macronutrient (but limited Fe content) ACC waters (Ito et al., 2005). At SSTC high primary productivity occurs and is evidenced from chlorophyll concentration elevation (Rasse et al., 2017). The warm and saline Brazil Current (BC, θ = 15–25 °C, S = 35–37) travels from the north along the western continental margin, while the Agulhas Current (AC, θ = 15–23 °C, $S > 35$) originates in the Indian Ocean and flows along the southern tip of Africa and then northwards near the eastern continental margin of Africa. Inshore from the Brazil Current at 54°W, salinity decreases to 28.5 due to freshwater discharge from the Rio de la Plata estuary (Fig. 4b).

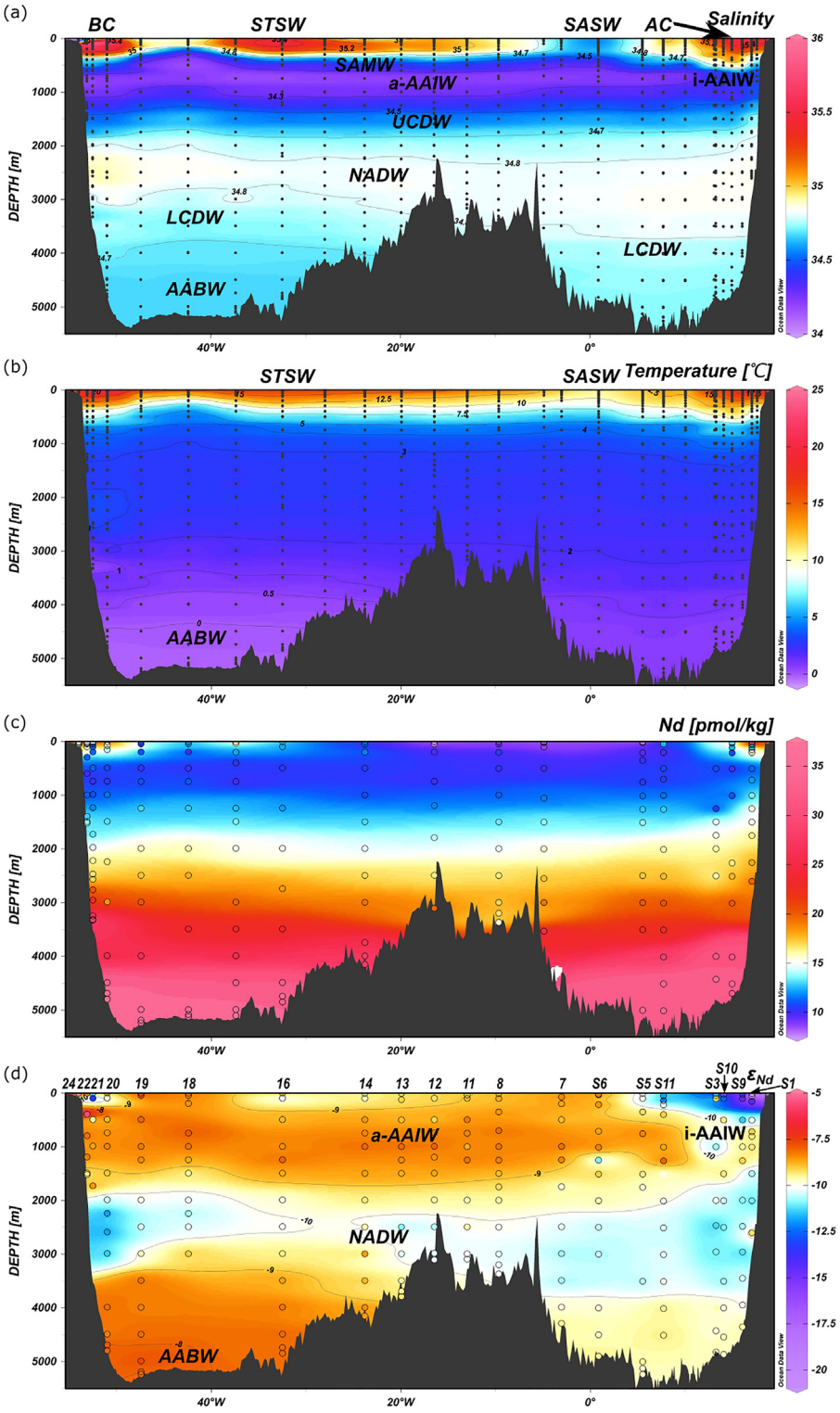

Fig. 2. Distribution profile along GA10 section of (a) Salinity, (b) Temperature, (c) Nd concentration, (d) ε_{Nd}. Data of temperature and salinity are from Wyatt et al. (2014). Data of Nd concentration is from The GEOTRACES IDP2017 (Schlitzer et al., 2017). These sections were created with Ocean Data View (Schlitzer, 2020).

At intermediate depths, northward flowing Subantarctic Mode Water (SAMW; characterized by high nitrate and low dissolved silica concentrations, Sarmiento et al., 2004) and Antarctic Intermediate Water (AAIW), with a salinity minimum ($S < 34.5$), lie at depths from ~300 to 600 m and 600 to 1400 m respectively. Both water masses form by sub-

duction of near surface water close to the Sub-Antarctic Front (Fig. 1a; Tsuchiya et al., 1994). Two varieties of AAIW can be recognized (Gordon et al., 1992; Garcia-Solsona et al., 2014): one formed in the South Atlantic Ocean (a-AAIW; S < 34.3); and one originating from the Indian Ocean (i-AAIW; S > 34.3). Upper Circumpolar Deep Water (UCDW) lies below AAIW between 1400 and 1800 m.

In the deep ocean, NADW (S > 34.75, ranging from 1800 m to ~3500 m) flows southward mainly with the Deep Western Boundary Current (DWBC) and a branch of it flows eastward when it reaches ~40°S. The majority of Lower Circumpolar Deep Water (LCDW) from the Pacific Ocean flows eastward at ~50°S through the Drake Passage, while a small portion of it flows northward along the western boundary of the Argentine Basin (Stramma and England, 1999). Below LCDW, the abyssal portion of the Argentine Basin and the Cape Basin is filled by colder and fresher northward flowing Weddell Sea Deep Water (WSDW). These two deep waters are together referred to as Antarctic Bottom Water (AABW).

2. MATERIAL AND METHODS

2.1. Sampling

Seawater samples from 20 depth profiles for Nd isotopic compositions and 17 profiles for REE concentrations were collected during GEOTRACES cruises D357 and JC068 (Fig. 1). Seawater samples with a volume of 5 or 10 L depending on availability and demand for ε_{Nd} analysis (and analyses for protactinium (Pa), thorium (Th) and uranium (U) isotopes) were drawn from Niskin bottles mounted on a CTD rosette into acid-cleaned polyethylene bottles after filtration through 0.45 μm AcroPak Supor® filters, following protocols suggested by GEOTRACES intercalibration work (Anderson et al., 2012). Similarly, ~250 ml seawater was drawn for Nd (and other REEs) concentration measurements. All samples were then acidified to pH ~1.7 with distilled concentrated HCl on board.

2.2. Analytical procedure

Seawater samples for ε_{Nd} analysis were initially processed using an iron (Fe) co-precipitation approach at the University of Oxford following Deng et al. (2014). After preconcentration by Fe co-precipitation, Pa, Th and U were separated and Nd was eluted with Fe from anion exchange chromatography and retained. The retained Nd was then purified at the University of Cambridge through three steps of column chemistry. REEs were separated from Fe using cation exchange chromatography (AG50W-X8, modified from Dausmann (2018)). The REEs were then separated from any remaining Fe and other matrix elements (e.g. Ba) using an additional smaller cation exchange column following the procedures of Greaves et al. (1989). Finally, Nd was separated from the other REEs using Eichrom LNspec™ resin (Wilson et al., 2012). Nd isotopes were measured on a Thermo Neptune Plus MC-ICP-MS with a 50 μl/min nebulizer at the University of Cambridge. A CETAC Aridus II desolvating sample introduction system and Jet/X Ni cones were used during analysis in order to maximize sensitivity for small sample sizes. Instrumental mass bias was corrected by normalizing $^{146}Nd/^{144}Nd$ to 0.7219 using the exponential law. Each sample was bracketed with analyses of JNdi-1 neodymium isotopic standard with a $^{143}Nd/^{144}Nd$ value corrected to 0.512115 ± 7 as reported by Tanaka et al. (2000). Further analytical details are presented in the Supplementary Information text 1.

REE and Nd concentrations were analysed at the University of Oxford, using an isotope dilution method described in Zheng et al. (2015). 250 ml samples were spiked with a mixture of enriched ^{145}Nd, ^{142}Ce and ^{171}Yb, preconcentrated using iron coprecipitation, and purified on a AG1-X8 column. Analyses were performed on the Thermo Scientific ELEMENT2 coupled with an Aridus I desolvator at the University of Oxford. Precision for all REE is <5% (2σ) and results for two uncertified seawater reference materials (CASS-4 & NASS-5) and GEOTRACES intercalibration samples agreed well with those reported from other laboratories (Zheng et al., 2015). Full results for the REE are publicly available in the GEOTRACES intermediate data products Mawji et al. (2014) and Schlitzer et al. (2017). Both ε_{Nd} and REE data conform to quality control imposed by the GEOTRACES programme.

3. RESULTS

Our ε_{Nd} data are reported for the first time, while REE data have been incorporated in the GEOTRACES Intermediate Data Product 2017 (IDP 2017; Schlitzer et al., 2017), but their oceanographic implications have not been discussed in any previous peer-reviewed literature. Here, we focus on the distribution of Nd concentrations and associated isotopic compositions.

The [Nd] generally increases with depth from the surface to deep ocean (from 7.6 to 36.9 pmol/kg, Fig. 2c) in open ocean stations (station S5 to 19) and varies similarly in the western (west of 10°W) and eastern (east of 10°W) South Atlantic. Higher [Nd] (up to 34.5 pmol/kg) is observed in the surface ocean near the continental margins (Fig. 2c).

Distribution of ε_{Nd}, shown in Fig. 2d, shows vertical and lateral variations across the section. In the surface ocean, ε_{Nd} ranges between −9 and −11 in the open sea. West to the continental margin of South America, ε_{Nd} becomes more radiogenic (~−7.5) alongside an increase in [Nd]. In the South American coastal currents at 54°W, ε_{Nd} reaches −4.49 (±0.15, 2SD). East to the continental margin of Southern Africa, ε_{Nd} is less radiogenic reaching −20.85 at 17°E (±0.28, 2SD) with elevated [Nd]. In the intermediate ocean, a-AAIW has distinct radiogenic ε_{Nd} values from −7.5 to −8.5 while i-AAIW has slightly less radiogenic ε_{Nd} values from −8.5 to −9.5. UCDW has a ε_{Nd} range between −8.5 to −11.0 and is more radiogenic on the western side when compared to the eastern side of the mid-ocean ridge. From 2000 to 3500 m, ε_{Nd} of NADW ranges between −9.5 to −11.9 along 40°S. In the abyssal layer, AABW in the Argentine Basin has more radiogenic

ε_{Nd} values (−7.6 to −10.0) than that measured in the Cape Basin (ε_{Nd} = −9.5 to −11.0).

4. DISCUSSION

4.1. Nd input to the surface ocean

Nd concentration increases in the surface ocean near the western and eastern continental margins (Fig. 3a, b and Fig. 4c). This could be explained by inputs of both dissolved and solid phases transported by rivers and ocean currents from nearby continents, as well as dust carried by wind (Frank, 2002). The continental input would raise [Nd], changing the shape of normalized REE patterns and ε_{Nd} values of surface waters, depending on how different the REE pattern and ε_{Nd} of input material is relative to seawater. The sole continent-derived input of Nd to the centre of the surface South Atlantic ocean is dust, primarily from the Puna-Central West Argentina region but dissolution of this dust is considered to be negligible (McGee et al., 2016).

4.1.1. Input to the western South Atlantic

When approaching the South American continental margin surface ocean, [Nd] increases from 7.8 to 34.5 pmol/kg (Fig. 3a and Fig. 4c). However, ε_{Nd} spatially varies in this high [Nd] area, largely following hydrography, indicating input from multiple sources. Nearshore at 54°W, ε_{Nd} of surface water is radiogenic (−4.5, JC068 Station 24) which is likely to reflect a signal of riverine discharge from the Rio de la Plata estuary due to the shallow depth (52 m) and low salinity (S = 28.5) of this sampling station. The ε_{Nd} value of dissolved load of tributaries varies from −5.6 to −12.1 (Henry et al., 1996). However, the ε_{Nd} signature at the mouth of the river is not constrained, such that the radiogenic ε_{Nd} value of surface water in the Rio de la Plata estuary may also be from the other unconstrained sources. Offshore from the Rio de la Plata estuary, surface to subsurface waters become less radiogenic (ε_{Nd} = −8.2 to −13.2, JC068 Station 22-20) within the Brazil Current. The most negative ε_{Nd} value corresponds to the centre of very saline subsurface water along the margin (Fig. 4b, d

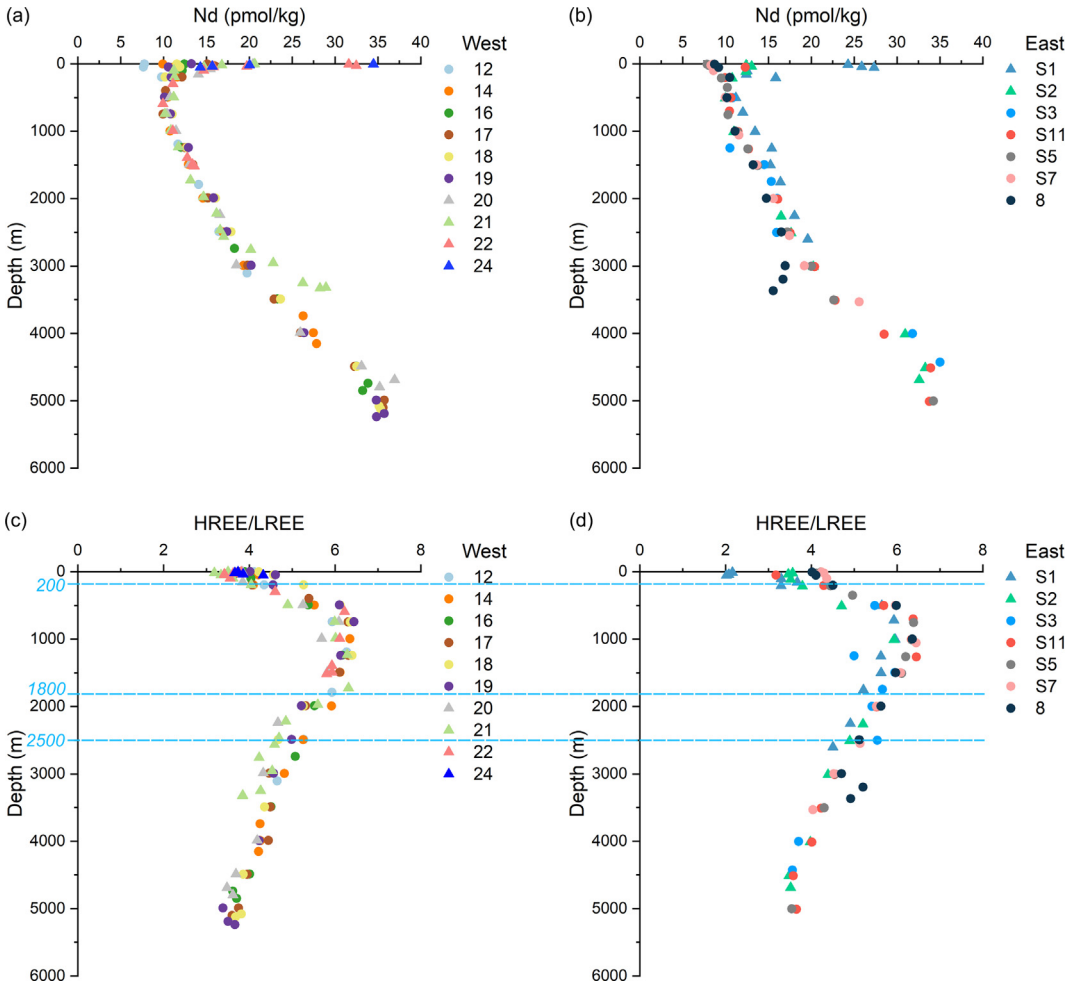

Fig. 3. Profiles of Nd concentrations of stations on (a) west and (b) east side of the Mid-Atlantic Ridge, and HREE/LREE ratio of stations on (c) west and (d) east side. Color-coding represents different stations and triangle denotes the stations near the margins. HREE/LREE = $(Tm_N + Yb_N + Lu_N)/(La_N + Pr_N + Nd_N)$ where subscript $_N$ denotes all elements are normalized to PAAS (Taylor and McLennan, 1985). Blue lines accord to the depth boundaries of four trajectories in Fig. 6. Data from The GEOTRACES IDP2017 (Schlitzer et al., 2017). (For interpretation of the references to color in this figure legend, the reader is referred to the web version of this article.)

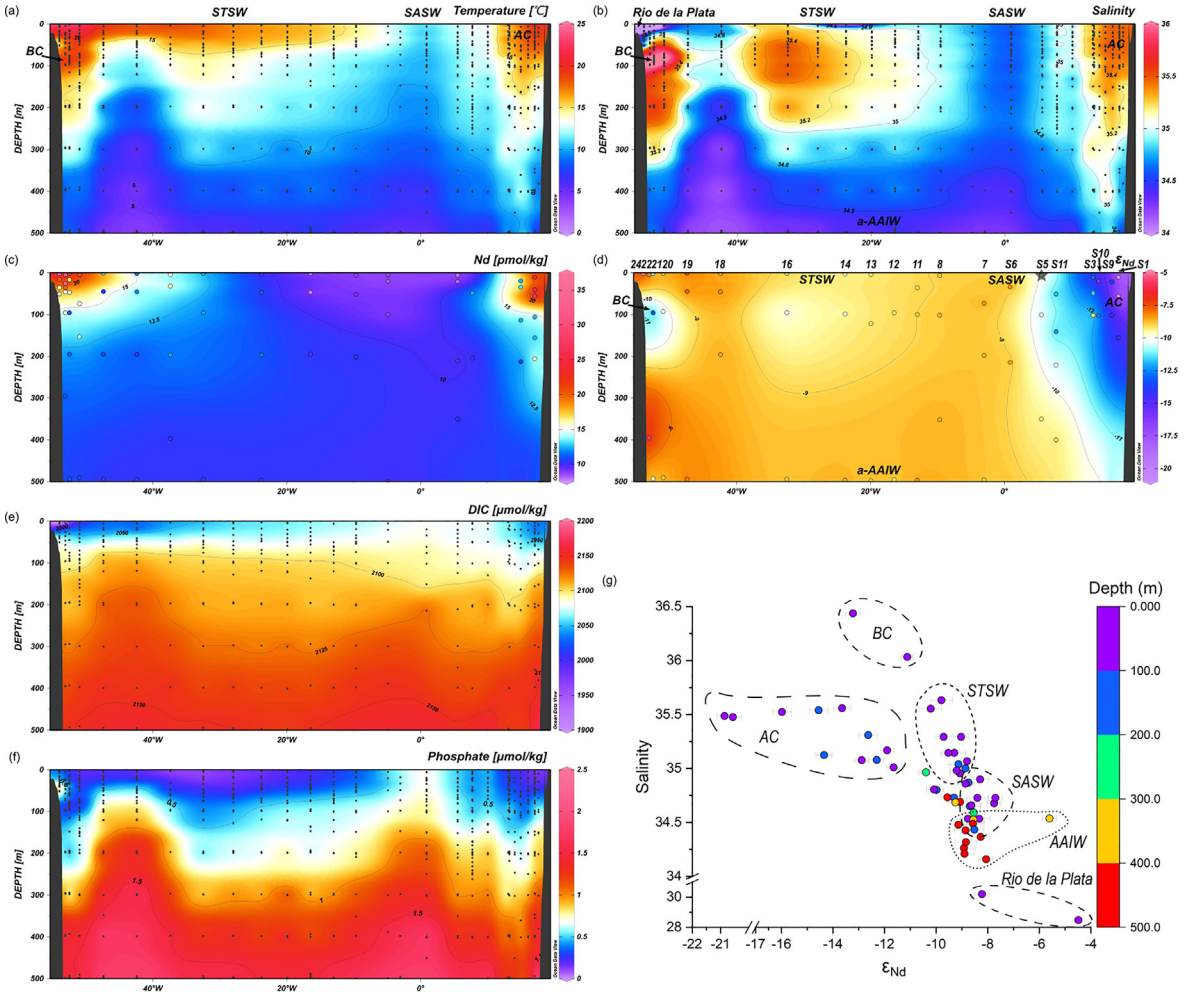

Fig. 4. Surface and subsurface ocean (0–500 m) distribution profile along GA10 section of (a) Temperature, (b) Salinity, (c) Nd concentration, (d) ε_{Nd}, (e) DIC concentration and (f) phosphate concentration, and (g) cross-plot of salinity to ε_{Nd}. Data of temperature, salinity and phosphate concentration are from Wyatt et al. (2014). Data of Nd and DIC concentration are from The GEOTRACES IDP2017 (Schlitzer et al., 2017). These sections were created with Ocean Data View (Schlitzer, 2020).

and g). This could be a result of the Nd release from upper margin sediments originating from the land of the Southeastern to Southern Brazil (average $\varepsilon_{Nd} = -13.0 \pm 2.1$ and -9.3 ± 0.9, respectively; de Mahiques et al.. 2008) or dust input from São Paulo ($\varepsilon_{Nd} = \sim -14$; Khondoker et al., 2018) carried by the southward Brazil Current to this location.

East of the Brazil Current from 50°W to 30°W, Nd concentration is still high in the surface layer relative to the underlying waters (Fig. 4c). This may be the result of surface outflow from Rio de la Plata estuary as mirrored by relatively lower salinities and more radiogenic ε_{Nd} values. It could also be a contribution from aeolian dust input and the most likely source is Patagonian desert (Johnson et al., 2011). However, the dust deposition and likely the amount of dissolution of this dust is relatively low compared to the North Atlantic under Sahara dust plume (Jickells et al., 2005; Deng et al., 2014). Moreover, the variation of ε_{Nd} of the surface waters between 50°W to 30°W follows the distribution of water masses (Fig. 4d and 4 g), indicating only a minor influence of a single input derived from dust dissolution ($\varepsilon_{Nd} = -2 \sim +1$; Gaiero et al., 2007).

The relatively radiogenic ε_{Nd} values and low salinities in the subsurface seawaters (below 100 m) at JC068 station 19 and 18 around 45°W (Fig. 4d) are similar to the signature of AAIW at intermediate depth, which coincides with elevated concentrations of DIC (Fig. 4e) and phosphate (Fig. 4f) as well as relatively colder waters (Fig. 4a). This could be a result of active cyclonic mesoscale eddy driven upwelling of deeper, colder, and nutrient-enriched waters, the occurrence of which is supported by depressed sea surface height observed by satellite altimetry during the time period of sampling (Browning et al., 2014).

4.1.2. Input to the eastern South Atlantic

Near the coast of South Africa, ε_{Nd} becomes progressively less radiogenic (reaching ε_{Nd} of −20.8 at 17°E, Fig. 4d) with increasing [Nd] (Fig. 4c). To estimate the average ε_{Nd} value of external source (ε_{Nd}^{input}), the following equation is used:

$$\varepsilon_{Nd}^{input} = \frac{\varepsilon_{Nd}^{final} * [Nd]^{final} - \varepsilon_{Nd}^{initial} * [Nd]^{initial}}{[Nd]^{final} - [Nd]^{initial}}$$

where "initial" denotes the composition of the water without influence from the input, and "final" refers to the water altered by the continental contribution. We consider surface water from D357 Station 5 (6 m, [Nd] = 7.9 pmol/kg, $\varepsilon_{Nd} = -10.08 \pm 0.28$, marked with a star at the surface of S5 column on Fig. 4d) as the "initial" value as it is the closest surface water with no obviously increased [Nd] relative to subsurface waters (101 m with $\varepsilon_{Nd} = -9.99 \pm 0.28$, and 211 m with [Nd] = 9.5 pmol/kg). In the absence of scavenging, the increased [Nd] would be equivalent to the Nd flux, which would require an input with ε_{Nd}^{input} of −26.0 and can be considered the lowest possible value. Therefore, the Nd input must be within the range of −26 to −20.8 (the measured value).

Previous studies have suggested that the ε_{Nd} value of surface water in nearby regions ($\varepsilon_{Nd} = -17.6$, Rahlf et al., 2020; $\varepsilon_{Nd} = -18.9$, Stichel et al., 2012; $\varepsilon_{Nd} = -17.1$, Garcia-Solsona et al., 2014) was due to partial dissolution of suspended sediments from the Orange River and the Agulhas current carrying old continental material from the eastern coast of South Africa. Orange River sediment, which has a similar Nd isotopic composition ($\varepsilon_{Nd} = -13.5$ to ~−24, n = 3; Reid et al., 1987), is dispersed westwards and northwards along the coast (Bluck et al., 2007) away from our sampling stations. The spatial pattern of ε_{Nd} which we measured (Fig. 4d) better matches the high salinity and temperature (Fig. 4a, b) of the Agulhas current, rather than the Orange River outflow, which is characterised by low salinity. Therefore, we suggest the negative ε_{Nd} values observed in the eastern South Atlantic surface water samples are transported by Agulhas leakage. The negative ε_{Nd} signal is likely originated from the Archaean Kaapvaal Craton (Chavagnac et al., 2001; Garcia-Solsona et al., 2014) which has an average ε_{Nd} value of −35.8 and thus sets the unradiogenic composition of dissolved load in the river to the coastal waters ($\varepsilon_{Nd} = -22.4$ at the Limpopo River mouth, Rahlf et al., 2020). This composition is within the range of possible Nd source compositions that we calculated above.

4.1.3. Decoupling of Nd concentration and isotopic composition in the surface ocean

The distribution of ε_{Nd} in the surface ocean matches the pattern of surface ocean hydrography near the margins, where spatial changes in Nd isotopes conform to the structure of the Brazil Current and Agulhas Current but differ from the more uniform composition of the open ocean (Fig. 4b, d and g). However, in the surface ocean [Nd] is high near both west and east continental margins due to continental inputs, and it is otherwise lower and more uniform laterally in the open ocean. The decoupling of distribution of [Nd] and ε_{Nd} in the surface ocean is best seen by the mismatch in patterns shown in Fig. 4c and d. We interpret this decoupling to be the result of REE scavenging onto particles in surface layers, producing a tilted "seawater-like" REE pattern (Fig. S2) with low LREE and high HREE as we observed in surface water masses. [Nd] is decreased by scavenging before it was homogenized in the surface ocean by mixing processes. The scavenging process preferentially removes LREEs from surrounding seawater onto particle surfaces but it does not fractionate Nd isotopes, such that ε_{Nd} follows hydrography and reflects the various sources of continental inputs. This means that ε_{Nd} has potential to be a water-mass tracer in the surface ocean away from the areas influenced by strong local Nd sources.

4.2. Nd cycling

4.2.1. Horizontal advection vs. vertical transport

To distinguish the relative importance of horizontal advection and vertical transport on Nd concentrations and isotope distributions at different depths in the South Atlantic, we apply a simple mixing model with prescribed water mass endmember compositions. In the deep ocean, two major endmembers considered in our model are lower-NADW (l-NADW, Lambelet et al., 2016) and AABW (Fig. 2). In the intermediate ocean, upper-NADW (u-NADW, Lambelet et al., 2016) and a-AAIW are two major water masses influencing our section, while i-AAIW exists only on the east side of the mid-ocean ridge. Due to the lack of endmember data in literature for i-AAIW and water masses in the surface ocean, we only constrained water mass proportions between l-NADW and AABW for the whole deep ocean (>2500 m), and u-NADW and a-AAIW for the west side of the intermediate ocean (600–2500 m). The endmember compositions are listed in Table 1 and the details on selection of endmember values are provided in the supplementary (text 2). Water mass mixing curves for salinity (S, a conservative parameter), [Nd] and ε_{Nd} are calculated as follows:

$$S_{Mix} = S_1 * f + S_2 * (1 - f) \quad (1)$$

$$[Nd]_{Mix} = [Nd]_1 * f + [Nd]_2 * (1 - f) \quad (2)$$

$$\varepsilon_{Nd}^{mix} = \frac{[Nd]_1 * \varepsilon_{Nd}^1 * f + [Nd]_2 * \varepsilon_{Nd}^2 * (1 - f)}{[Nd]_1 * f + [Nd]_2 * (1 - f)} \quad (3)$$

where the subscript number denotes a water mass (Table 1). S_{Mix}, $[Nd]_{Mix}$ and ε_{Nd}^{mix} are the salinity, [Nd] and ε_{Nd} values of mixture of two sourced endmembers, and f is the fraction of a water mass in the mixture, which we assigned values from 0 to 1 with 0.1 (10%) increments.

The resulting mixing envelopes are plotted in Fig. 5 against our measured data. On the west side of the intermediate ocean (Fig. 5a) between 600 to 2500 m, [Nd] is close to the value predicted from conservative mixing with a slight excess below ~2000 m showing the importance of horizontal water mass advection in controlling chemical compositions at this depth. However, [Nd] increases with depth at a ratio higher than what would be the case from only water mass mixing, and, accordingly, the Nd isotopic composition has been modified to more radiogenic values (indicated by orange arrows in Fig. 5a and b). This indicates the influence of a more radiogenic source, likely a-AAIW overlying u-NADW, through a vertical process. A similar process may also operate on the east side of the intermediate ocean where less radiogenic i-AAIW contribution deviates the

Table 1
Water mass end members of the Atlantic Ocean.

Water mass	Salinity	1SD	T (°)	1SD	Depth (m)	1SD	n	Reference
a-AAIW	34.254	0.053	3.71	0.56	897	126	18	This study
upper-NADW	35.036	0.088	4.43	0.77	1544	435	29	Schmittner et al. (2013); Lambelet et al. (2016)
lower-NADW	34.930	0.018	2.78	0.19	3095	722	7	
AABW	34.674	0.024	0.01	0.50	3954	640	11	Tachikawa et al. (2017)

Water mass	[Nd] (pmol/kg)	1SD	n	εNd	1SD	n	Reference
a-AAIW	10.7	0.5	8	−8.28	0.26	7	This study
upper-NADW	17.6	0.6	10	−13.20	0.50	10	Lambelet et al. (2016)
lower-NADW	22.5	4.1	16	−12.40	0.20	10	
AABW	26.1	1.3	11	−8.40	0.46	11	Tachikawa et al. (2017)

a-AAIW end member is selected between 700–1000 m (core of a-AAIW) from this study due to the vicinity to its origin and lack of data in previous studies.

data to a different direction (indicated by blue arrows in Fig. 5d). The vertical process is likely to be similar in intensity in both western and eastern Atlantic due to similar productivity (Rasse et al., 2017). This is supported by similar REE distributions (Fig. 3).

In the deep ocean, however, Nd concentrations can show −10 and +10 pmol/kg offsets, while Nd isotopic compositions follow the conservative mixing envelope. This decoupling of Nd concentrations and isotopic compositions, where concentration increases with depth while Nd isotopes trace the water mass mixing, is a good example of the so-called "Nd paradox". To better understand this decoupling, we need to investigate the vertical processes in the study area first.

4.2.2. Vertical processes of Nd

[Nd] increases smoothly with depth at a rate of ~3 pmol/kg per km from ~800 m to 2000 m, and a higher rate of ~8 pmol/kg per km below 3000 m (Fig. 3a and b), except for two stations influenced by benthic processes (JC068 Station 8 and 21, discussed in 4.2.2.4). The increase indicates that reversible scavenging exists below the euphotic zone to the bottom of the ocean (Siddall et al., 2008; Rempfer et al., 2011; Stichel et al., 2020). To better understand the vertical processes transporting Nd from shallower depths to the deeper ocean, the types of particles controlling the vertical transport and depth of release need to be discussed.

The high productivity in the euphotic layer around SSTC produces a large number of organic particles (POC) that can scavenge Nd and other REEs. As these particles settle, they carry REEs to the deep ocean, which can be then released during reversible scavenging or during particle dissolution at depths. When organic particles dissolve, they consume dissolved oxygen, increasing the apparent oxygen utilization (AOU). AOU is defined as the difference between observed oxygen concentration and saturated oxygen concentration in water with the same physical and chemical properties at a given depth. To elucidate vertical [Nd] distribution influenced by scavenging and remineralization of organic matter, we followed the approach used in Stichel et al. (2015) to plot Nd concentrations against AOU as a function of water depth (Fig. 6). AOU increases when decomposition of organic matter consumes oxygen, which has been suggested to be accompanied by an increase in [REE] because organic particles can release previously scavenged REEs when they decompose (van de Flierdt et al., 2016). This diagram provides a way to infer whether a change in [Nd] is related to formation and remineralization of organic particles, or scavenging and release from inorganic particles. According to the data assemblage, we divided the [Nd] vs. AOU plot into four parts by depth (see "pathways" A, B, C and D in Fig. 6). Trajectories "A" and "D" occurring in the shallowest and deepest sites are similar to what was found by Stichel et al. (2015), while Trajectories "B" and "C" are new.

4.2.2.1. Trajectory "A" – Scavenging. Trajectory "A" is found in the euphotic layer (0–200 m) where [Nd] decreases dramatically at a constant AOU. The consumed oxygen is quickly resupplied due to exchange with the atmosphere, resulting in low, sometimes even negative, AOU values. The decrease of [Nd] with low AOU can be interpreted as scavenging onto biogenic particle as they form or scavenging onto dust particles. However, the [Nd] decrease in our location (from 35 to ~7.5 pmol/kg) is even greater than what was observed in the Eastern North Atlantic (from 26 to 12 pmol/kg; Stichel et al., 2015) under the Saharan dust plume. Moreover, the [Nd] structure with depth, with higher [Nd] in the surface layer and lower [Nd] in the subsurface layer, suggests higher input at the surface layers followed by higher scavenging and adsorption in areas of elevated biological productivity. This is especially true in the high productivity SSTC zone (Rasse et al., 2017) (Fig. 1a). Therefore, compared to the areas with large dust input (e.g., the tropical Atlantic underneath Sahara dust belt), the major control of lowering [Nd] in the euphotic zone in the subtropical South Atlantic appears to be biogenic particle formation (Owens et al., 2015; Rasse et al., 2017). The scavenging in the euphotic layer across the whole section is indicated by the increasing trend of HREE/LREE ratio (Fig. 3c and d).

4.2.2.2. Trajectory "B" – Decomposition of organic particles. Below the euphotic layer to ~1800 m (trajectory "B", in Fig. 6), [Nd] increases with rising AOU. The positive linear

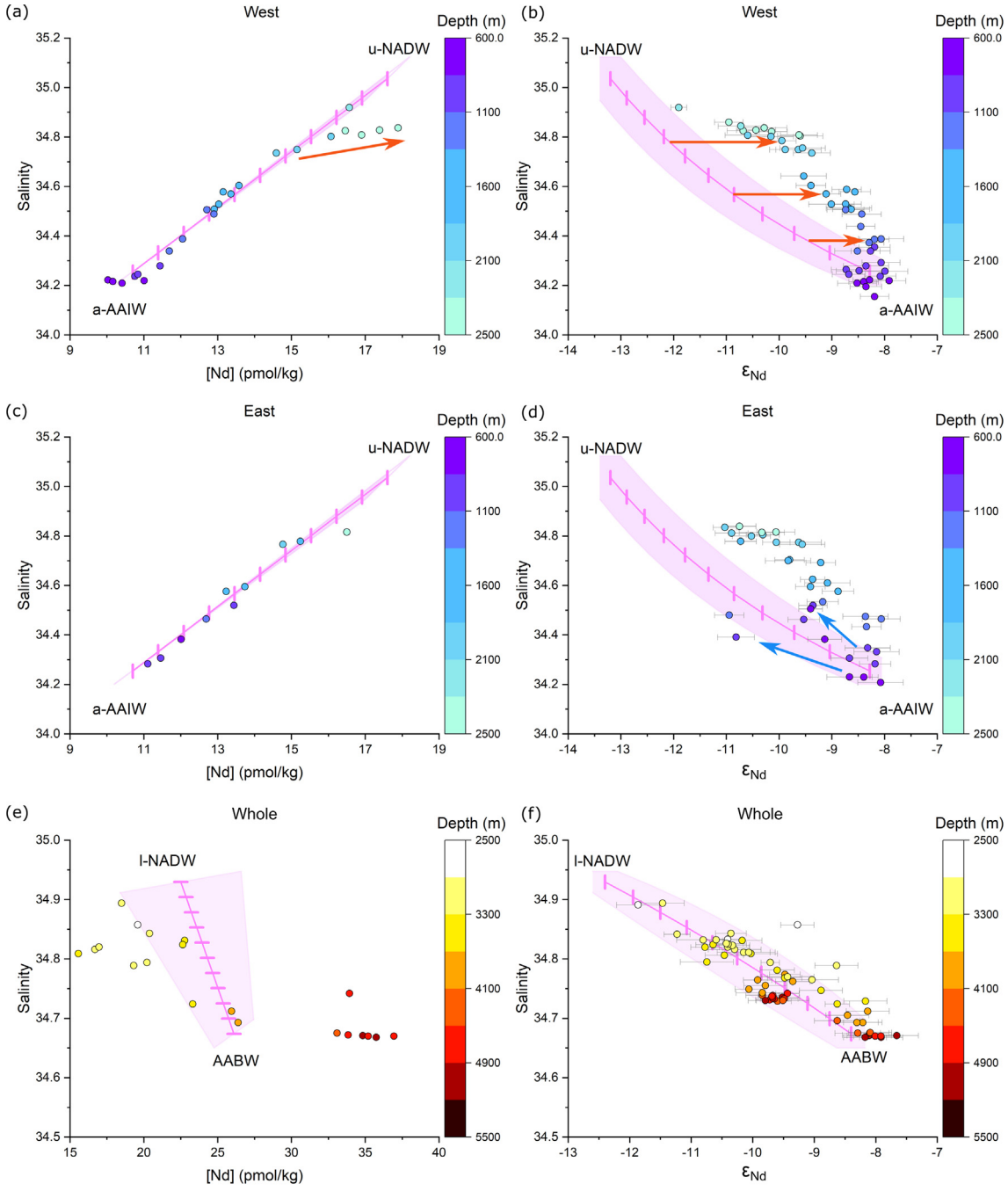

Fig. 5. Cross-plots of salinity-[Nd] and salinity- ε_{Nd} with conservative mixing curve of (a) (b) intermediate ocean of western Atlantic, (c) (d) intermediate ocean of eastern Atlantic, and (e) (f) whole deep ocean, respectively. Color-coding represents water depth. Orange arrows in (a) (b) and blue arrows in (d) indicate the offset from conservative mixing. (For interpretation of the references to color in this figure legend, the reader is referred to the web version of this article.)

correlation between [Nd] and AOU is high ($R^2 = 0.84$), suggesting that the decomposition of organic particles releases Nd back to the surrounding water. The release rate is ~3 pmol/kg per 100 μmol/kg AOU. The net release of [Nd] in the South Atlantic causes seawater concentration to increase by 3–4 pmol/kg in trajectory "B" which is low compared to the decrease in surface ocean concentration by scavenging (~27 pmol/kg). This [Nd] increase is low compared to trajectory "B" under the Saharah Dust Plume (Stichel et al., 2015) which has a ratio of ~5 pmol/kg Nd release per 100 μmol/kg AOU. A number of possibilities could explain the lower [Nd]/AOU ratio, including (1) high re-scavenging, (2) water mass distribution, and (3) an overestimation of AOU, which we will discuss in turn.

Further evidence for reversible exchange comes from variations in HREE/LREE ratios. The HREE/LREE

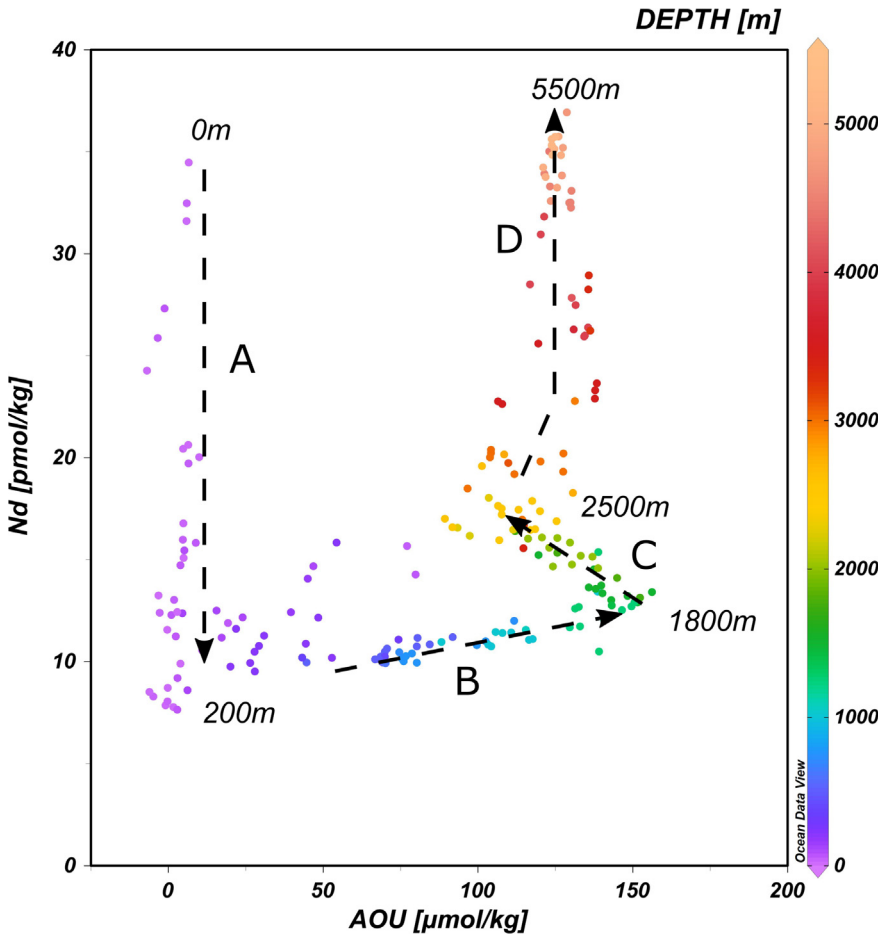

Fig. 6. [Nd] as a function of apparent oxygen utilization (AOU). Color-coding represents water depth. Arrows represent the different trajectories of changes in [Nd] (A: scavenging in the euphotic layer, B: upper water column remineralization, C: water mass mixing and reversible scavenging underneath oxygen minimum zone, D: water mass mixing and deep ocean release). Data from The GEOTRACES IDP2017 (Schlitzer et al., 2017). (For interpretation of the references to color in this figure legend, the reader is referred to the web version of this article.)

increases with depth in the euphotic zone, where particles are produced, and in fact continues to increase to proximate 800 m depth (Fig. 3c and d). During scavenging LREE are preferentially scavenged to particles, increasing the HREE/LREE of water. Therefore, the increasing HREE/LREE with depth suggests that scavenging continues to occur despite the lack of production of new organic bioparticles below the euphotic zone. This can be reconciled by "net scavenging" (i.e., scavenging minus desorption) continuing to occur to 800 m. Another contributor to the increased HREE/LREE between 200 and 800 m is the release by remineralization of opal. Lagarde et al. (2020) observed enrichment of HREE over LREE, as well as negative Ce anomaly, in the authigenic phase in areas of high biological productivity and attributed it to the biogenic silica. The remineralization of such particulates will decrease Ce/Ce*, increase both [Nd] and HREE/LREE ratio of the dissolved phase, as the same influence as scavenging on Nd concentration but the opposite on the REE ratio. This remineralization release likely stops at ~800 m where Ce/Ce* in the dissolved phase does not decrease and becomes constant (Fig. S3), mirrors the increase of Ce/Ce* in the particulates as observed by Lagarde et al. (2020). Between 800 and 1200 m depth, the scavenging versus desorption reaches to a balance where HREE/LREE ratio retains constant (Fig. 3c and d). Scavenging becomes lower than desorption from ~1200 m to the bottom ocean. The depth offset of the "turning point" between Nd vs. AOU (Fig. 6) and HREE/LREE (Fig. 3c and d) indicates that besides organic influences there are other non-organic particles involved in scavenging/desorption. The Nd which is released from decomposition of organic particles is re-scavenged onto non-organic particles. This leads to the appearance that [Nd] is increasing with depth while AOU is rising. This demonstrates that reversible scavenging process happens not only in the surface ocean but also at deeper depths, implying a transfer of Nd isotopic compositions from shallower to deeper waters.

A second possible explanation for the difference is water mass distribution. Trajectory B encompasses SAMW (~300 to 600 m) and AAIW (600–1400 m) which are characterised by their temperature and salinity and have distinct pre-

formed biogeochemical properties as a function of the biological productivity at the sea surface. The GA10 section closely neighbours the formation region of both SAMW and AAIW (SAF; Tsuchiya et al., 1994), so is sensitive to the preformed compositions. In particular, low [Nd] due to high scavenging in shallower depth could contribute to the low [Nd]/AOU ratio (Hathorne et al., 2015). Nevertheless, this factor is likely to be minor because the strong correlation between [Nd] and AOU is consistent between 200 m and 1800 m, which goes deeper than the two different water masses.

Another possibility is that AOU is overestimated below ~400 m along 40°S as suggested by Ito et al. (2004), because the water masses formed from surface water in high latitude, i.e., AAIW and AABW in this study, are not at oxygen saturation level which leads to an overestimation of AOU. The overestimation above 1800 m is less than 30 μM (Ito et al., 2004) while the total change in Trajectory B is 150 μM. This might contribute to the [Nd]/AOU ratio but would not be the major control of the strong correlation of AOU-[Nd].

4.2.2.3. Trajectory "C" – Vertical transport and horizontal advection. From ~1800 m to ~2500 m (trajectory "C", in Fig. 6), [Nd] increases with rising oxygen concentration. This change corresponds to the core of upper NADW with higher oxygen content and slightly higher [Nd]. Meanwhile, HREE/LREE ratio decreases within this depth interval (Fig. 3c and d), indicating that more desorption occurs than scavenging. As suggested in 4.2.1 and Fig. 5, ε_{Nd} has been modified to more radiogenic compositions by vertical transport from shallow to deeper waters, while [Nd] does not show obvious elevation. We suggest that it is a result of reversible exchange that the re-scavenging decreases [Nd] after the release and isotopic equilibrium in the dissolved phase. In this case, both vertical process and horizontal water mass transfer control [Nd].

The release in this water depth interval is no longer caused by organic decomposition because the AOU decreases. Instead, we suggest that non-biogenic particles such as lithogenic and authigenic particles play an important role.

4.2.2.4. Trajectory "D" – Deep ocean release. Below ~2500 m (trajectory "D", in Fig. 6), [Nd] increases with depth at a generally constant AOU, indicating no obvious decomposition of organic materials in the deep ocean. There is a slight increase of AOU between 2500–3500 m which can be explained by the transition from NADW to AABW and the known overestimation of AOU in AABW (Ito et al., 2004). Similar to the water column above (1800–2500 m), both vertical process and horizontal water mass advection are believed to control [Nd].

As shown in Fig. 5e, Nd concentration is greatly depleted (-10 pmol/kg) above 3000 m and greatly enriched (+10 pmol/kg) below 4000 m relative to the concentration expected from conservative mixing of water masses (mixing curve between NADW and AABW end members). However, the Nd isotopic ratio conforms to the conservative mixing line (Fig. 5f). These indicate that non-conservative processes play a role here to dramatically change [Nd] but only slightly modify ε_{Nd}. Below we will discuss the possibility of processes that cause the "Nd paradox", including benthic processes ("bottom-up", from the sediment water interface) and/or reversible scavenging ("top-down", from sediments sinking from shallower depths).

Lack of evidence for benthic processes

Here we consider all the processes happening at the water-sediment interface (e.g., Haley et al., 2004; Abbott et al., 2015; Jeandel, 2016) and hydrothermal venting (e.g., Douville et al., 1999) as benthic processes since they affect bottom seawater Nd concentrations and isotopic compositions.

The coherency of REE concentrations, patterns, and Nd isotopic compositions is an argument against significant benthic input, which would be expected to dramatically change the REE pattern and HREE/LREE ratio of bottom seawater (e.g., Haley et al., 2004; Abbott et al., 2015). All rare earth elements increase with depth from 2500 m to the bottom of the ocean (Fig. 3a and b), for all the stations except JC068 Station 8 and 21, and the trend of decreasing HREE/LREE ratio with depth (Fig. 3c and d) and normal "seawater-type" REE pattern continues through the deep water column without any changes (Fig. S2). This indicates that the same processes continue to control REE patterns throughout the deep water column, and no significant benthic process or input affects the bottom water chemistry. This would include dissolution of detritus or previously formed coatings on the sediments. We do note that a slight decrease of [Nd] and an increase of HREE/LREE of the bottom-most sample compared with the sample above have been observed at many stations (Fig. 3a and b). This is not consistent with input of REE, but likely results from stronger removal of REE by scavenging near the water-sediment interface due to the elevated particle concentrations of benthic nepheloid layer (Fig. S4) (Gardner et al., 2018). Similarly, Station 8 shows lower concentration of REEs and higher HREE/LREE ratio approaching the bottom (Fig. 3b and d). Considering the station is right above the Mid-Atlantic Ridge (Fig. 2d), REEs of bottom seawaters in this location are scavenged by hydrothermal activity with a preferential scavenging on LREEs (Stichel et al., 2018). In contrast, Station 21 shows much higher REE concentrations and lower HREE/LREE ratios near the bottom of the profile (Fig. 3a and c). This could be a result of elevated depth of a water mass boundary or continental input at ~3000 m depth because of the vicinity to the continental margin (Fig. 2d). However, due to a lack of ε_{Nd} in deep ocean on this location, we cannot differentiate the reason for this increase, but if it is due to benthic input it is spatially confined to a small area. In either case, the signal at this local input is not obviously affected the isotopic composition of bottom waters due to lateral advection to become visible in neighbouring stations (Fig. 2d).

In conclusion, at sites away from the continental margins and mid-ocean ridge, benthic processes are negligible in setting [Nd] and ε_{Nd} in the deep South Atlantic. This differs from the argument presented in Rahlf et al. (2020), who attributed the observed excess [Nd] in the bottom seawater in the Cape Basin to particle dissolution.

Reversible scavenging

[Nd] increases almost linearly with depth, indicating the existence of reversible scavenging (Siddall et al., 2008; Stichel et al., 2020). It is also noteworthy that the process we observed here is not a single-step of scavenging at the surface ocean and release at depth, because this would result in Nd concentration exceeding the value brought horizontally by the deep water mass end members. Instead, our observation shows that Nd concentration is much lower than the end member water mass concentrations above 3000 m (Fig. 7c), indicating that re-scavenging is occurring, i.e. it is a reversible exchange. This means that vertically (1) particles sink down with scavenged Nd from the upper water column; (2) Nd desorption and equilibrium in seawater; (3) particles re-scavenge Nd and sink to deeper depths.

The influence of desorption on seawater could be complicated due to various types of particles and by what triggers the exchange processes, but we can rule out some processes as being dominant. The dissolution of detrital particles, for example, would release a large amount of REEs and change the REE pattern and HREE/LREE ratios in the resulting seawater, but no such change has been observed so it is unlikely to be a dominant process.

4.2.3. Particles controlling the vertical processes

The transmissometer beam attenuation (TBA) data (Fig. S4) show that the amount of particles is high (TBA reaches to ~0.3 m^{-1}) in the euphotic zone (0–100 m) and in the deep ocean especially along the margin of South America along deep western boundary current and at abyssal depth (>4500 m). The high amount of particle in the surface ocean is due to high biogenic productivity and perhaps some dust input, while at the bottom depths it is likely to be nepheloid layers resulting from benthic storms. From 100 m to 4500 m depth, the amount of particles as indicated by transmissometer beam attenuation (0–0.15 m^{-1}) is largely uniform.

Stichel et al. (2020) collected suspended particles in the North Atlantic and measured their components. They showed that the fraction of particulate organic matter (POM), biogenic opal, and $CaCO_3$ generally decreases with depth at stations where dissolved Nd concentration increases with depth. Meanwhile, the fraction of $Fe(OH)_2$, MnO_2, and lithogenic material increases with depth at those stations. In our study location, biogenic opal only accounts for a very small fraction (Pichevin et al., 2014) that is less likely to control the vertical processes. The close coupling of [Nd] and AOU at shallow depths suggests that POM dominates scavenging and release of dissolved REEs in the euphotic layer and until ~1800 m depth, respectively. Below 1800 m, there are only few organic particles and those exist are large aggregates and faecal pellets which rapidly sink to the bottom (Poulton et al., 2006). Therefore, any reversible scavenging in the deep and abyssal ocean is likely to be controlled by inorganic particles.

Bayon et al. (2004) highlighted the influence of preformed Fe-Mn oxyhydroxides carried by aeolian particles from nearby Namib Desert into the North Cape Basin, near our transect. The REEs are firstly being released from these easily leached components of the dust and then re-scavenged on to the particles due to the reprecipitation of Fe-Mn oxyhydroxides in the deep ocean. Schijf et al. (2015) also pointed out that the REE scavenging in the deep ocean is dominated by hydrated Mn oxide particles. This is likely to be important in our study area due to obvious aeolian input from Patagonian dust into the southwest Atlantic (Johnson et al., 2011) and dust from Puna-Central West Argentina region into the centre South Atlantic (McGee et al., 2016). The reprecipitation of metal oxides can occur below the oxygen minimum zone, re-scavenging the REEs from ambient seawater.

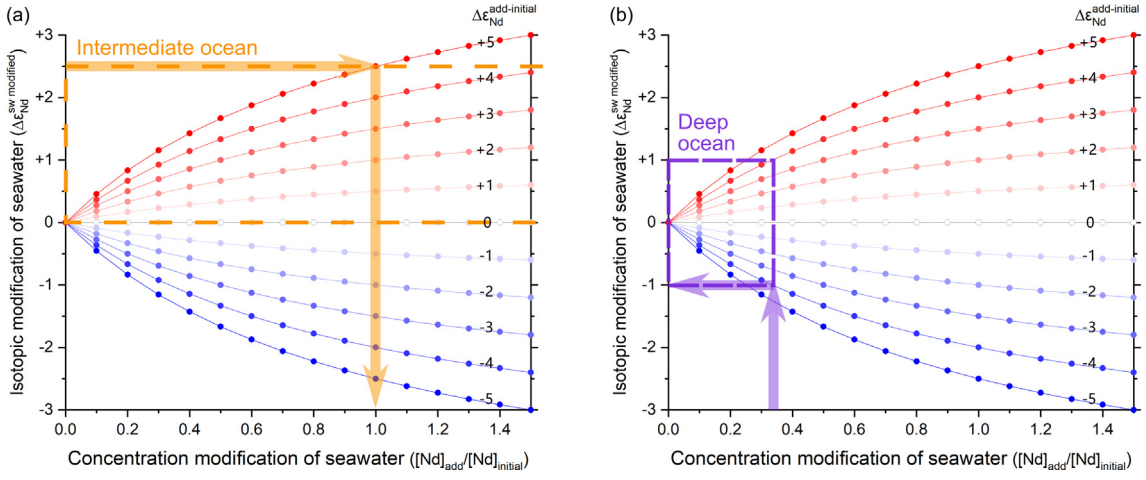

Fig. 7. Sensitivity test of seawater ε_{Nd} modified by the release of Nd in (a) the intermediate ocean and (b) the deep ocean. The x-axis is the concentration modification of seawater due to vertical processes that equal to the concentration ratio of increased Nd to initial Nd in the ambient seawater ($[Nd]_{add}/[Nd]_{initial}$); the y-axis is the isotopic modification of seawater after the Nd addition. $\Delta\varepsilon_{Nd}^{add-initial}$ denotes the difference of ε_{Nd} value between additive Nd to initial Nd. Orange and purple boxes indicate the situation of intermediate and deep ocean, respectively. Arrows show the steps of calculation. (For interpretation of the references to color in this figure legend, the reader is referred to the web version of this article.)

The windblown and current transported fine fraction is largely composed of clay minerals, which can also control adsorption/desorption of dissolved REEs as they disaggregate/aggregate (or dissolve). However, in contrast to most particle surfaces, clay minerals preferentially adsorb HREEs because of their surface chemistry (Aagaard, 1974; Coppin et al., 2002). In this case, the adsorption and desorption process will decrease and increase HREE/LREE ratio of seawater, respectively, which is the opposite of what we observe. Therefore, the reversible scavenging process is unlikely to be controlled by clay minerals in our study area. At the same time, we cannot exclude the potential release of REE from clay which has undergone partial dissolution.

Other types of particles, i.e., $CaCO_3$ and authigenic particles, may also be important in controlling the vertical REE transport. Further determination of the roles that different types of particles play should be ascertained by analyses of suspended particulate matter lithology, surface chemistry, and particle size in the South Atlantic.

4.3. Decoupled behaviour of Nd concentrations and isotopic compositions in the South Atlantic

Siddall et al. (2008) and Rempfer et al. (2011) suggested that the degree of congruence in the spatial pattern of ε_{Nd} and salinity is dependent on reversible scavenging and the efficiency of downward transport of Nd by settling particles. Their models took efforts to match the global-scale distribution of [Nd] and ε_{Nd} in all ocean basins by advection and reversible scavenging. Here we take a different approach by examining the relationship of [Nd] and ε_{Nd} across intermediate and deep ocean water mass boundaries using a sensitivity test and observations of horizontal and vertical concentrations and compositions.

We consider particles falling through the water column are the main source and sink of Nd, and the exchangeable Nd on their surfaces is derived from shallower water masses. While we cannot differentiate the exchange processes which occur within our transect relative to the those which have already occurred between deep water formation and arrival at our transect, the lateral continuity of major water masses like AAIW, NADW, and AABW means that the vertical isotopic transport is the same over large areas. Therefore we take an Atlantic Ocean basin-scale view and suggest that the isotopic modification of seawater due to vertical processes ($\Delta\varepsilon_{Nd}^{swmodified}$, y axis in Fig. 7) is related to the amount of Nd added ($[Nd]_{add}/[Nd]_{initial}$, x axis) and the isotopic composition from particle falling through the water column while they reversibly exchange (different curves in Fig. 7). The curves are calculated using:

$$\Delta\varepsilon_{Nd}^{swmodified} = \frac{[Nd]_{initial} * \varepsilon_{Nd}^{initial} + [Nd]_{add} * \varepsilon_{Nd}^{add}}{[Nd]_{initial} + [Nd]_{add}} - \varepsilon_{Nd}^{initial} \quad (4)$$

The difference between ε_{Nd} of previously scavenged Nd and the initial seawater ε_{Nd}, which reflects only conservative changes in ε_{Nd} due to water mass mixing is $\Delta\varepsilon_{Nd}^{add-initial}$. This ranges from −5 to +5 depending on the difference between an water mass end member and the water mass below it (i.e., from a-AAIW to NADW is about −5, and from NADW to AABW is about +5, Table 1).

4.3.1. Vertical cycling at intermediate depths

The Nd isotopic compositions between 600 m to 2500 m are shifted from the initial conservative values towards more radiogenic values, up to +2.5 ε_{Nd} (upper NADW Fig. 5b). Above 600 m lies a-AAIW which contains the most radiogenic ε_{Nd} value in the water column. We suggest that the offset at 600–2500 m is the result of Nd previously scavenged from a-AAIW onto particles and transported to depth to be released. The needed concentration elevation for the isotopic modification in u-NADW can be calculated following equation (4). For example, we take +2.5 ε_{Nd} modification (the maximum isotopic change at 600–2500 m) and the maximum $\Delta\varepsilon_{Nd}^{add-initial}$ of +5 (ε_{Nd} difference between a-AAIW and u-NADW). Our calculation (see arrows in Fig. 7a) shows that [Nd] must be increased to two times relative to the conservative [Nd] ($[Nd]_{add}/[Nd]_{initial} = 1.0$) caused by mixing between these two water masses. Re-scavenging subsequently lowers this concentration enrichment without changing the isotopic composition. The elevated [Nd] should be higher when $\Delta\varepsilon_{Nd}^{add-initial}$ is less than +5. Therefore, the scenario of the intermediate ocean is signified by the open orange box in Fig. 7a.

It is hard to constrain the exact amount of released Nd because there is uncertainty about the isotopic composition which is being released from the particles. However, it seems to be the case that the re-scavenging process removes the excess Nd in the intermediate depth, causing the final [Nd] to return to similar initial [Nd] as that from conservative mixing. This is possibly because the amount of release and re-scavenging are both controlled by the particle surface area. However, the Nd isotopic composition of the water is modified by the release from the particles, and the modification is not affected as re-scavenging occurs. This reversible scavenging process results in an appearance that the seawater Nd isotopic composition is dramatically modified while the concentration is not obviously elevated. Global ocean modelling by Siddall et al. (2008) suggested that when sinking particles enter a new water mass with similar Nd concentration but different ε_{Nd}, the particles exchange isotopes without altering Nd concentrations. The variations in Nd isotopes, concentration and REE patterns in our South Atlantic data are consistent with this being the dominant process.

4.3.2. The insensitivity of ε_{Nd} change in the deep ocean and its relationship to the "Nd paradox"

Below 2500 m, non-conservative vertical processes affect the Nd concentration profile while ε_{Nd} follows the water mass distribution (Fig. 5e and 5f). We use the same sensitivity test as in Section 4.3.1 (Eq. (4)) to illustrate why, unlike intermediate waters, the Nd isotopic composition of deep waters is insensitive to desorptive addition of Nd from particles. Because the Nd isotopic compositions of advected waters range from −8 to −12 below 2500 m in our study area (e.g NADW and AABW) and reversible scavenging means that particles are continuously scavenging and

releasing these compositions as they fall through the deep water, the $\Delta\varepsilon_{Nd}^{add-initial}$ at these depths ranges from +4 to −4. To assess the isotopic modification of seawater due to vertical processes, we make an example calculation for AABW at our study section, which has a Nd concentration of 36.9 pmol/kg, as $[Nd]_{final}$ (= $[Nd]_{initial}$ + $[Nd]_{add}$) and the initial conservative [Nd] of AABW (26.1 pmol/kg) as $[Nd]_{initial}$. Then $[Nd]_{add}/[Nd]_{initial}$ is less than 40% and the maximum of $\Delta\varepsilon_{Nd}^{add-initial}$ is −1.0 indicated by arrows in Fig. 8b. The curves (a. 7b purple box, signifying deep ocean) indicate the scenario in the deep ocean and shows that that $\Delta\varepsilon_{Nd}^{swmodified}$ is nearly always less than an epsilon unit, because the added [Nd] is small relative to the $[Nd]_{initial}$. An offset of one epsilon unit is usually within the scatter of data around the conservative mixing envelope, as well as the errors of possible endmember values for water masses (Fig. 5f). This means that, because the southern-sourced water mass (i.e., AABW) has a high [Nd] endmember composition, the vertical cycling of a given amount of Nd from shallower water masses into it does not effectively change its Nd isotopic composition. This causes a decoupling between isotopic composition and concentration (Fig. 5e and f) relative to the conservative mixing curves which are based on global or regional endmembers leading to the appearance that there is much larger change in Nd concentration than for Nd isotopes. This is the key to answering the "Nd paradox".

The insensitivity of the change in bottom seawater Nd isotopic composition to non-conservative input was also reported by Rahlf et al. (2020) in the Cape Basin. Our interpretation of our data shows that this effect can be seen across the South Atlantic, independent of zonal changes along the section in biological productivity, upwelling, and boundary currents.

4.4. Global Ocean "Nd paradox

In the deep South Atlantic Ocean, the decoupling of Nd concentrations and isotopic compositions (i.e., the Nd paradox) is explained by the reversible scavenging and the high [Nd] in the deep-water mass relative to the reversible exchange [Nd]. To examine whether this effect can be seen in other ocean basins, here we, based on available observational data, did the same water mass mixing model and sensitivity test as was carried out for the South Atlantic in Section 4.3.2.

For the Atlantic Ocean we used the same water mass endmembers, i.e., l-NADW and Atlantic sector AABW (a-AABW), for the mixing model in the Atlantic Ocean. Fig. 8a and b show the observation data of the North Atlantic and the South Atlantic relative to the conservative mixing curve. Similar to our observation in the South Atlantic, most isotopic data in the North Atlantic follow the mixing curve while the concentration data do not. The isotopic modification is more obvious in the North Atlantic due to slightly lower [Nd] of NADW (Fig. 8c). The proximity to the formation area of NADW precursors (Greenland Sea and Labrador Sea water masses) also contributes to greater scatter than in the South Atlantic. Nevertheless, our sensitivity test is similar throughout the North and South Atlantic Ocean, suggesting that reversible scavenging causes decoupling of [Nd] and ε_{Nd} throughout the Atlantic. This is not surprising because AABW with a high [Nd] fills much of the abyssal Atlantic.

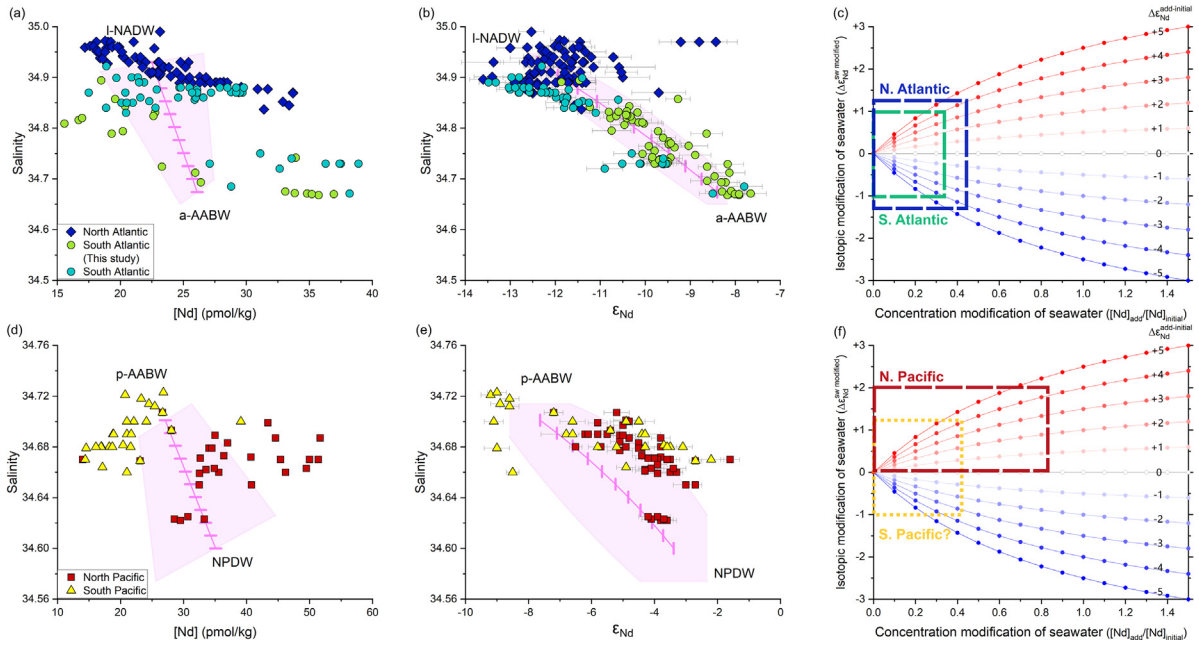

Fig. 8. Global Ocean seawater Nd data and sensitivity test: cross-plot of (a) salinity-[Nd] and (b) salinity- ε_{Nd} with conservative mixing curve, and (c) sensitivity test of the whole Atlantic Ocean; cross-plot of (d) salinity-[Nd] and (e) salinity- ε_{Nd} with conservative mixing curve, and (f) sensitivity test of the whole Pacific Ocean.

Pacific AABW (p-AABW) and North Pacific Deep Water (NPDW) are the major water mass endmembers in the deep Pacific (Table S3). In the North Pacific, Nd concentrations are generally higher than should be the case from conservative mixing, while Nd isotopic compositions are ~2.5 epsilon unit more radiogenic than the conservative mixing curve (Fig. 8d and e). For the maximum elevated [Nd] (~28 pmol/kg to ~52 pmol/kg) and a difference between NPDW and p-AABW of +4.2 ε_{Nd}, we calculate that the modified ε_{Nd} should be about +2 (Fig. 8f), which is less than the observed change (up to +4 ε_{Nd}). Therefore, other non-conservative processes such as benthic input likely contribute to modification of ε_{Nd} to more radiogenic values in the North Pacific as suggested by other studies (e.g. Haley et al., 2004; Abbott et al., 2015). In the South Pacific, however, [Nd] is lower than that expected from conservative mixing, while ε_{Nd} has been modified more dramatically. This indicates that re-scavenging is occurring after isotopic modification from other non-conservative processes (Goldstein and Hemming, 2003). Though it is not possible to calculate the amount of Nd added because we do not know how much re-scavenging occurred, it is noteworthy that the data lie along the conservative mixing curve. It appears that in the Atlantic and South Pacific, which are filled with southern-sourced deep waters (AABW), reversible scavenging on falling particles is not a strong enough process to the homogenize the isotopic composition in the deep waters, though do change the concentration, producing the Nd paradox.

5. CONCLUSION

The water mass profile of Nd in the subtropical South Atlantic is dominated by horizontally conservative water mass mixing at all depths, but vertically non-conservative processes, such as reversible scavenging, are important especially for modifying the Nd concentration. Nd is input to the surface ocean from continental detritus in the western South Atlantic from riverine (Rio de la Plata), continental shelf (carried by Brazil Current), and aeolian (Patagonian dust) sources, resulting in high Nd concentrations and spatially variable Nd isotopic compositions in the surface ocean. Input into the eastern South Atlantic surface ocean at 40°S is mainly derived from old continental crust and is carried by the Agulhas Current, causing it to have a less radiogenic ε_{Nd} value (-20.8). Nd concentration is high at the sea surface and decreases to minimum above ~200 m due to the rapid scavenging of surface ocean Nd onto biogenic organic particles. At intermediate depth (~200 to 2500 m), Nd is released by particulate organic oxidation and decomposition and then is likely re-scavenged onto non-organic particles, therefore acting non-conservatively. There is also a greater dominance of horizontal water mass mixing with depth. In the deep ocean (>2500 m), ε_{Nd} is dominated by the mixing of water masses, however [Nd] is modified by release and re-scavenging by non-biogenic particles as they fall through the water column. The ε_{Nd} is less sensitive than Nd concentration changes during vertical cycling in the deep ocean because Nd already has a high preformed concentration in southern-sourced water masses (e.g. AABW). This results in a decoupling of Nd concentrations and isotopic compositions relative to mixing between major water mass endmembers, which has been termed the "Nd Paradox". Our observations indicate that Nd isotopes are less modified by vertical processes than Nd concentrations in the deep South Atlantic Ocean, and by extension other areas of the global deep ocean. Because Antarctic-derived waters with high preformed Nd concentrations fill the global deep ocean, we suggest that reversible scavenging results in the so-called "Nd Paradox" throughout much of the ocean. Therefore, Nd isotopes can be utilized as a quasi-conservative proxy to trace present-day deep ocean circulation and, with adequate knowledge of past endmember isotopic compositions, concentrations, and post-depositional processes, can be used to reconstruct deep ocean circulation in the past.

Declaration of Competing Interest

The authors declare that they have no known competing financial interests or personal relationships that could have appeared to influence the work reported in this paper.

ACKNOWLEDGEMENT

The authors thank the captain, officers, crew, and scientific party during the UK GEOTRACES Legs D357 and JC068. We also specifically thank Gideon M. Henderson for organising the UK GEOTRACES effort, being chief scientist on Legs D357 and JC068, and for being lead PI on NERC Consortium grant (NE/H008713/1) "Ocean Micronutrient Cycles: UK GEOTRACES" and acknowledge the support of NERC through this Consortium grant. We thank Victoria Rennie for analysis of some initial samples at University of Cambridge. X.-Y. Zheng acknowledges support from US National Science Foundation (Award 2049554). Ruixue Wang is supported by CSC Cambridge International Scholarship jointly funded by Cambridge TRUST and China Scholarship Council. We also thank three anonymous reviewers and the editor, Tina van de Flierdt, for their insightful and helpful comments which greatly improved this manuscript.

APPENDIX A. SUPPLEMENTARY MATERIAL

Supplementary data to this article can be found online at https://doi.org/10.1016/j.gca.2021.09.015.

REFERENCES

Aagaard P. (1974) Rare earth elements adsorption on clay minerals. *Bull. du Groupe français des argiles* **26**, 193–199.

Abbott A. N., Haley B. A. and McManus J. (2015) Bottoms up: Sedimentary control of the deep North Pacific Ocean's εNd signature. *Geology* **43**, 1035–1038.

Amakawa H., Sasaki K. and Ebihara M. (2009) Nd isotopic composition in the central North Pacific. *Geochim. Cosmochim. Acta* **73**, 4705–4719.

Amakawa H., Yu T. L., Tazoe H., Obata H., Gamo T., Sano Y., Shen C. C. and Suzuki K. (2019) Neodymium concentration and isotopic composition distributions in the southwestern Indian Ocean and the Indian sector of the Southern Ocean. *Chem. Geol.* **511**, 190–203.

Anderson R. F., Fleisher M. Q., Robinson L. F., Edwards R. L., Hoff J. A., Moran S. B., van der Loeff M. R., Thomas A. L., Roy-Barman M. and Francois R. (2012) GEOTRACES intercalibration of 230 Th, 232 Th, 231 Pa, and prospects for 10 Be. *Limnol. Oceanogr. Methods* **10**, 179–213.

Bayon G., German C. R., Burton K. W., Nesbitt R. W. and Rogers N. (2004) Sedimentary Fe-Mn oxyhydroxides as paleoceanographic archives and the role of aeolian flux in regulating oceanic dissolved REE. *Earth Planet. Sci. Lett.* **224**, 477–492.

Bluck B. J., Ward J. D., Cartwright J. and Swart R. (2007) The Orange River, southern Africa: An extreme example of a wave-dominated sediment dispersal system in the South Atlantic Ocean. *J. Geol. Soc. Lond.* **164**, 341–351.

Browning T. J., Bouman H. A., Moore C. M., Schlosser C., Tarran G. A., Woodward E. M. S. and Henderson G. M. (2014) Nutrient regimes control phytoplankton ecophysiology in the South Atlantic. *Biogeosciences* **11**, 463–479.

Byrne R. H. and Kim K. H. (1990) Rare earth element scavenging in seawater. *Geochim. Cosmochim. Acta* **54**, 2645–2656.

Chavagnac V., Kramers J. D., Nägler T. F. and Holzer L. (2001) The behaviour of Nd and Pb isotopes during 2.0 Ga migmatization in paragneisses of the Central Zone of the Limpopo Belt (South Africa and Botswana). *Precambr. Res.* **112**, 51–86.

Coppin F., Berger G., Bauer A., Castet S. and Loubet M. (2002) Sorption of lanthanides on smectite and kaolinite. *Chem. Geol.* **182**, 57–68.

Deng F., Thomas A. L., Rijkenberg M. J. A. and Henderson G. M. (2014) Controls on seawater 231Pa, 230Th and 232Th concentrations along the flow paths of deep waters in the Southwest Atlantic. *Earth Planet. Sci. Lett.* **390**, 93–102.

Dausmann V. (2018) Present and past changes in continental weathering and ocean circulation from radiogenic Nd, Hf and Pb isotopes. (Doctoral dissertation).

Douville E., Bienvenu P., Charlou J.-L., Donval J.-P., Fouquet Y., Appriou P. and Gamo T. (1999) Yttrium and rare earth elements in fluids from various deep-sea hydrothermal systems - evidence for heat extraction from magma chambers or cracking fronts? *Geochem. Cosmochem. Acta* **63**, 627–643.

Elderfield H., Whitfield M., Burton J. D., Bacon M. P. and Liss P. S. (1988) The oceanic chemistry of the rare-earth elements. *Philos. Trans. R. Soc. A Math. Phys. Eng. Sci.* **325**, 105–126.

Farmer J. R., Hönisch B., Haynes L. L., Kroon D., Jung S., Ford H. L., Raymo M. E., Jaume-Seguí M., Bell D. B., Goldstein S. L., Pena L. D., Yehudai M. and Kim J. (2019) Deep Atlantic Ocean carbon storage and the rise of 100,000-year glacial cycles. *Nat. Geosci.* **12**, 355–360.

van de Flierdt T., Grifths A. M., Lambelet M., Little S. H., Stichel T. and Wilson D. J. (2016) Neodymium in the oceans: A global database, a regional comparison and implications for palaeoceanographic research. *Philos. Trans. R. Soc. A Math. Phys. Eng. Sci.* **374**, 20150293.

Frank M. (2002) Radiogenic isotopes: Tracers of past ocean circulation and erosional input. *Rev. Geophys.* **40**, 1–1.

Fuhr M., Laukert G., Yu Y., Nürnberg D. and Frank M. (2021) Tracing water mass mixing from the equatorial to the North Pacific Ocean with dissolved neodymium isotopes and concentrations. *Front. Mar. Sci.* **7**, 1–18.

Gaiero D. M., Brunet F., Probst J. L. and Depetris P. J. (2007) A uniform isotopic and chemical signature of dust exported from Patagonia: Rock sources and occurrence in southern environments. *Chem. Geol.* **238**, 107–120.

Garcia-Solsona E., Jeandel C., Labatut M., Lacan F., Vance D., Chavagnac V. and Pradoux C. (2014) Rare earth elements and Nd isotopes tracing water mass mixing and particle-seawater interactions in the SE Atlantic. *Geochim. Cosmochim. Acta* **125**, 351–372.

Gardner W. D., Richardson M. J. and Mishonov A. V. (2018) Global assessment of benthic nepheloid layers and linkage with upper ocean dynamics. *Earth Planet. Sci. Lett.* **482**, 126–134.

Goldstein S. L. and Hemming S. R. (2003) Long-lived isotopic tracers in oceanography, paleoceanography, and ice-sheet dynamics. *Treatise Geochem.* **6**, 625.

Goldstein S. L., O'Nions R. K. and Hamilton P. J. (1984) A SmNd isotopic study of atmospheric dusts and particulates from major river systems. *Earth Planet. Sci. Lett.* **70**, 221–236.

Gordon A. L., Weiss R. A. Y. F., Smethie W. M. and Warner M. J. (1992) Thermocline and intermediate water communication between the South Atlantic and Indian Oceans. *J. Geophys. Res. Ocean.* **97**, 7223–7240.

Grasse P., Stichel T., Stumpf R., Stramma L. and Frank M. (2012) The distribution of neodymium isotopes and concentrations in the Eastern Equatorial Pacific: Water mass advection versus particle exchange. *Earth Planet. Sci. Lett.* **353–354**, 198–207.

Greaves M. J., Elderfield H. and Klinkhammer G. P. (1989) Determination of the rare earth elements in natural waters by isotope-dilution mass spectrometry. *Anal. Chim. Acta* **218**, 265–280.

Haley B. A., Klinkhammer G. P. and McManus J. (2004) Rare earth elements in pore waters of marine sediments. *Geochim. Cosmochim. Acta* **68**, 1265–1279.

Hathorne E. C., Stichel T., Brück B. and Frank M. (2015) Rare earth element distribution in the Atlantic sector of the Southern Ocean: The balance between particle scavenging and vertical supply. *Mar. Chem.* **177**, 157–171.

Henry F., Probst J. L., Thouron D., Depetris P. and Garçon V. (1996) Nd-Sr isotopic compositions of dissolved and particulate material transported by the Parana and Uruguay rivers during high (December 1993) and low (September 1994) water periods. / Compositions isotopiques de Nd et Sr des matières en suspension et dissout. *Sci. Géologiques. Bull.* **49**, 89–100.

Ito T., Follows M. J. and Boyle E. A. (2004) Is AOU a good measure of respiration in the oceans? *Geophys. Res. Lett.* **31**, 1–4.

Ito T., Parekh P., Dutkiewicz S. and Follows M. J. (2005) The Antarctic circumpolar productivity belt. *Geophys. Res. Lett.* **32**.

Jeandel C. (2016) Overview of the mechanisms that could explain the "Boundary Exchange" at the land-ocean contact. *Philos. Trans. R. Soc. A Math. Phys. Eng. Sci.* **374**, 20150287.

Jickells T. D., An Z. S., Andersen K. K., Baker A. R., Bergametti C., Brooks N., Cao J. J., Boyd P. W., Duce R. A., Hunter K. A., Kawahata H., Kubilay N., LaRoche J., Liss P. S., Mahowald N., Prospero J. M., Ridgwell A. J., Tegen I. and Torres R. (2005) Global iron connections between desert dust, ocean biogeochemistry, and climate. *Science* **308**, 67–71.

Johnson M. S., Meskhidze N., Kiliyanpilakkil V. P. and Gassó S. (2011) Understanding the transport of Patagonian dust and its influence on marine biological activity in the South Atlantic Ocean. *Atmos. Chem. Phys.* **11**, 2487–2502.

Khondoker R., Weiss D., van de Flierdt T., Rehkämper M., Kreissig K., Coles B. J., Strekopytov S., Humphreys-Williams E., Dong S., Bory A., Bout-Roumazeilles V., Smichowski P., Cid-Agüero P., Babinski M., Losno R. and Monna F. (2018) New constraints on elemental and Pb and Nd isotope compositions of South American and Southern African aerosol sources to the South Atlantic Ocean. *Chem. Erde* **78**, 372–384.

Lacan F. and Jeandel C. (2005) Neodymium isotopes as a new tool for quantifying exchange fluxes at the continent-ocean interface. *Earth Planet. Sci. Lett.* **232**, 245–257.

Lagarde M., Lemaitre N., Planquette H., Grenier M., Belhadj M., Lherminier P. and Jeandel C. (2020) Particulate rare earth element behavior in the North Atlantic (GEOVIDE cruise). *Biogeosciences* **17**, 5539–5561.

Lambelet M., van de Flierdt T., Crocket K., Rehkämper M., Kreissig K., Coles B., Rijkenberg M. J. A., Gerringa L. J. A., de Baar H. J. W. and Steinfeldt R. (2016) Neodymium isotopic composition and concentration in the western North Atlantic Ocean: Results from the GEOTRACES GA02 section. *Geochim. Cosmochim. Acta* **177**, 1–29.

de Mahiques M. M., Tassinari C. C. G., Marcolini S., Violante R. A., Figueira R. C. L., da Silveira I. C. A., Burone L. and de Mello e Sousa S. H. (2008) Nd and Pb isotope signatures on the Southeastern South American upper margin: Implications for sediment transport and source rocks. *Mar. Geol.* **250**, 51–63.

Mawji E., Schlitzer R., Dodas E. M., Abadie C., Abouchami W., Anderson R. F., Baars O., Bakker K., Baskaran M., Bates N. R., Bluhm K., Bowie A., Bown J., Boye M., Boyle E. A., Branellec P., Bruland K. W., Brzezinski M. A., Bucciarelli E., Buesseler K., Butler E., Cai P., Cardinal D., Casciotti K., Chaves J., Cheng H., Chever F., Church T. M., Colman A. S., Conway T. M., Croot P. L., Cutter G. A., De Baar H. J. W., De Souza G. F., Dehairs F., Deng F., Dieu H. T., Dulaquais G., Echegoyen-Sanz Y., Lawrence Edwards R., Fahrbach E., Fitzsimmons J., Fleisher M., Frank M., Friedrich J., Fripiat F., Galer S. J. G., Gamo T., Solsona E. G., Gerringa L. J. A., Godoy J. M., Gonzalez S., Grossteffan E., Hattaa M., Hayes C. T., Heller M. I., Henderson G., Huang K. F., Jeandel C., Jenkins W. J., John S., Kenna T. C., Klunder M., Kretschmer S., Kumamoto Y., Laan P., Labatut M., Lacan F., Lam P. J., Lannuzel D., Le Moigne F., Lechtenfeld O. J., Lohan M. C., Lua Y., Masqué P., McClain C. R., Measures C., Middag R., Moffett J., Navidad A., Nishioka J., Noble A., Obata H., Ohnemus D. C., Owens S., Planchon F., Pradoux C., Puigcorbé V., Quaya P., Radic A., Rehkämper M., Remenyi T., Rijkenberg M. J. A., Rintoul S., Robinson L. F., Roeske T., Rosenberg M., Van Der Loeff M. R., Ryabenko E., Saito M. A., Roshan S., Salt L., Sarthou G., Schauer U., Scott P., Sedwick P. N., Sha L., Shiller A. M., Sigman D. M., Smethie W., Smith G. J., Sohrin Y., Speich S., Stichel T., Stutsman J., Swift J. H., Tagliabue A., Thomas A., Tsunogai U., Twining B. S., Van Aken H. M., Van Heuven S., Van Ooijen J., Van Weerlee E., Venchiarutti C., Voelker A. H. L., Wake B., Warner M. J., Woodward E. M. S., Wu J., Wyatt N., Yoshikawa H., Zheng X. Y., Xue Z., Zieringer M. and Zimmer L. A. (2014) The GEOTRACES Intermediate Data Product 2014. *Mar. Chem.* **177**, 1–8.

McGee D., Winckler G., Borunda A., Serno S., Anderson R. F., Recasens C., Bory A., Gaiero D., Jaccard S. L., Kaplan M., McManus J. F., Revel M. and Sun Y. (2016) Tracking eolian dust with helium and thorium: Impacts of grain size and provenance. *Geochim. Cosmochim. Acta* **175**, 47–67.

Molina-Kescher M., Frank M. and Hathorne E. (2014) South Pacific dissolved Nd isotope compositions and rare earth element distributions: Water mass mixing versus biogeochemical cycling. *Geochim. Cosmochim. Acta* **127**, 171–189.

Oka A., Tazoe H. and Obata H. (2021) Simulation of global distribution of rare earth elements in the ocean using an ocean general circulation model. *J. Oceanogr.* **77**, 413–430.

Owens S. A., Pike S. and Buesseler K. O. (2015) Thorium-234 as a tracer of particle dynamics and upper ocean export in the Atlantic Ocean. *Deep Res. Part II Top. Stud. Oceanogr.* **116**, 42–59.

Pichevin L. E., Ganeshram R. S., Geibert W., Thunell R. and Hinton R. (2014) Silica burial enhanced by iron limitation in oceanic upwelling margins. *Nat. Geosci.* **7**, 541–546.

Piepgras D. J. and Jacobsen S. B. (1988) The isotopic composition of neodymium in the North Pacific. *Geochim. Cosmochim. Acta* **52**, 1373–1381.

Piepgras D. J. and Wasserburg G. J. (1982) Isotopic composition of neodymium in waters from the Drake Passage. *Science* **217**, 207–214.

Piotrowski A. M., Goldstein S. L., Hemming S. R. and Fairbanks R. G. (2005) Temporal relationship of carbon cycling and ocean circulation at glacial boundaries. *Science* **307**, 1933–1938.

Poulton A. J., Sanders R., Holligan P. M., Stinchcombe M. C., Adey T. R., Brown L. and Chamberlain K. (2006) Phytoplankton mineralization in the tropical and subtropical Atlantic Ocean. *Glob. Biogeochem. Cycles* **20**, 1–10.

Rahlf P., Hathorne E., Laukert G., Gutjahr M., Weldeab S. and Frank M. (2020) Tracing water mass mixing and continental inputs in the southeastern Atlantic Ocean with dissolved neodymium isotopes. *Earth Planet. Sci. Lett.* **530** 115944.

Rasse R., Dall'Olmo G., Graff J., Westberry T. K., van Dongen-Vogels V. and Behrenfeld M. J. (2017) Evaluating optical proxies of particulate organic carbon across the surface Atlantic ocean. *Front. Mar. Sci.* **4**, 1–18.

Reid D. L., Erlank A. J., Welke H. J. and Moyes A. (1987) The Orange River Group: a major Proterozoic calcalkaline volcanic belt in the western Namaqua Province, southern Africa. *Geol. Soc. Lond. Spec. Publ.* **33**, 327–346.

Rempfer J., Stocker T. F., Joos F., Dutay J. C. and Siddall M. (2011) Modelling Nd-isotopes with a coarse resolution ocean circulation model: Sensitivities to model parameters and source/sink distributions. *Geochim. Cosmochim. Acta* **75**, 5927–5950.

Sarmiento J. L., Gruber N., Brzezinski M. A. and Dunne J. P. (2004) High-latitude controls of thermocline nutrients and low latitude biological productivity. *Nature* **427**, 56–60.

Schijf J., Christenson E. A. and Byrne R. H. (2015) YREE scavenging in seawater: A new look at an old model. *Mar. Chem.* **177**, 460–471.

Schlitzer R. (2020) Ocean Data View Available at: https://odv.awi.de, .

Schlitzer R., Anderson R. F., Dodas E. M., Lohan M., Geibert W., Tagliabue A., Bowie A., Jeandel C., Maldonado M. T., Landing W. M., Cockwell D., Abadie C., Abouchami W., Achterberg E. P., Agather A., Aguliar-Islas A., van Aken H. M., Andersen M., Archer C., Auro M., de Baar H. J., Baars O., Baker A. R., Bakker K., Basak C., Baskaran M., Bates N. R., Bauch D., van Beek P., Behrens M. K., Black E., Bluhm K., Bopp L., Bouman H., Bowman K., Bown J., Boyd P., Boye M., Boyle E. A., Branellec P., Bridgestock L., Brissebrat G., Browning T., Bruland K. W., Brumsack H.-J., Brzezinski M., Buck C. S., Buck K. N., Buesseler K., Bull A., Butler E., Cai P., Mor P. C., Cardinal D., Carlson C., Carrasco G., Casacuberta N., Casciotti K. L., Castrillejo M., Chamizo E., Chance R., Charette M. A., Chaves J. E., Cheng H., Chever F., Christl M., Church T. M., Closset I., Colman A., Conway T. M., Cossa D., Croot P., Cullen J. T., Cutter G. A., Daniels C., Dehairs F., Deng F., Dieu H. T., Duggan B., Dulaquais G., Dumousseaud C., Echegoyen-Sanz Y., Edwards R. L., Ellwood M., Fahrbach E., Fitzsimmons J. N., Russell Flegal A., Fleisher M. Q., van de Flierdt T., Frank M., Friedrich J., Fripiat F., Fröllje H., Galer S. J. G., Gamo T., Ganeshram R. S., Garcia-Orellana J., Garcia-Solsona E., Gault-Ringold M., George E., Gerringa L. J. A., Gilbert M., Godoy J. M., Goldstein S. L., Gonzalez S. R., Grissom K., Hammerschmidt C., Hartman A., Hassler C. S., Hathorne E. C., Hatta M., Hawco N., Hayes C. T., Heimbürger L.-E., Helgoe J., Heller M., Henderson G. M., Henderson P. B., van Heuven S., Ho P., Horner T. J., Hsieh Y.-T., Huang K.-F., Humphreys M. P., Isshiki K., Jacquot J. E., Janssen D. J., Jenkins W. J., John S., Jones E. M., Jones J. L., Kadko D. C., Kayser R., Kenna T. C., Khondoker R., Kim T., Kipp L., Klar J. K., Klunder M., Kretschmer S., Kumamoto

Y., Laan P., Labatut M., Lacan F., Lam P. J., Lambelet M., Lamborg C. H., Le Moigne F. A. C., Le Roy E., Lechtenfeld O. J., Lee J.-M., Lherminier P., Little S., López-Lora M., Lu Y., Masque P., Mawji E., Mcclain C. R., Measures C., Mehic S., Barraqueta J.-L. M., van der Merwe P., Middag R., Mieruch S., Milne A., Minami T., Moffett J. W., Moncoiffe G., Moore W. S., Morris P. J., Morton P. L., Nakaguchi Y., Nakayama N., Niedermiller J., Nishioka J., Nishiuchi A., Noble A., Obata H., Ober S., Ohnemus D. C., van Ooijen J., O'Sullivan J., Owens S., Pahnke K., Paul M., Pavia F., Pena L. D., Peters B., Planchon F., Planquette H., Pradoux C., Puigcorbé V., Quay P., Queroue F., Radic A., Rauschenberg S., Rehkämper M., Rember R., Remenyi T., Resing J. A., Rickli J., Rigaud S., Rijkenberg M. J. A., Rintoul S., Robinson L. F., Roca-Martí M., Rodellas V., Roeske T., Rolison J. M., Rosenberg M., Roshan S., Rutgers van der Loeff M. M., Ryabenko E., Saito M. A., Salt L. A., Sanial V., Sarthou G., Schallenberg C., Schauer U., Scher H., Schlosser C., Schnetger B., Scott P., Sedwick P. N., Semiletov I., Shelley R., Sherrell R. M., Shiller A. M., Sigman D. M., Singh S. K., Slagter H. A., Slater E., Smethie W. M., Snaith H., Sohrin Y., Sohst B., Sonke J. E., Speich S., Steinfeldt R., Stewart G., Stichel T., Stirling C. H., Stutsman J., Swarr G. J., Swift J. H., Thomas A., Thorne K., Till C. P., Till R., Townsend A. T., Townsend E., Tuerena R., Twining B. S., Vance D., Velazquez S., Venchiarutti C., Villa-Alfageme M., Vivancos S. M., Voelker A. H. L., Wake B., Warner M. J., Watson R., van Weerlee E., Alexandra Weigand M., Weinstein Y., Weiss D., Wisotzki A., Woodward E. M. S., Wu J., Wu Y., Wuttig K., Wyatt N., Xiang Y., Xie R. C., Xue Z., Yoshikawa H., Zhang J., Zhang P., Zhao Y., Zheng L., Zheng X.-Y., Zieringer M., Zimmer L. A., Ziveri P., Zunino P. and Zurbrick C. () The GEOTRACES Intermediate Data Product 2017. *Chem. Geol.* **493**, 210–223.

Schmittner A., Gruber N., Mix A. C., Key R. M., Tagliabue A. and Westberry T. K. (2013) Biology and air-sea gas exchange controls on the distribution of carbon isotope ratios ($\delta^{13}C$) in the ocean. *Biogeosciences* **10**, 5793–5816.

Siddall M., Khatiwala S., van de Flierdt T., Jones K., Goldstein S. L., Hemming S. and Anderson R. F. (2008) Towards explaining the Nd paradox using reversible scavenging in an ocean general circulation model. *Earth Planet. Sci. Lett.* **274**, 448–461.

Singh S. P., Singh S. K., Goswami V., Bhushan R. and Rai V. K. (2012) Spatial distribution of dissolved neodymium and εNd in the Bay of Bengal: Role of particulate matter and mixing of water masses. *Geochim. Cosmochim. Acta* **94**, 38–56.

Stichel T., Frank M., Rickli J. and Haley B. A. (2012) The hafnium and neodymium isotope composition of seawater in the Atlantic sector of the Southern Ocean. *Earth Planet. Sci. Lett.* **317–318**, 282–294.

Stichel T., Hartman A. E., Duggan B., Goldstein S. L., Scher H. and Pahnke K. (2015) Separating biogeochemical cycling of neodymium from water mass mixing in the Eastern North Atlantic. *Earth Planet. Sci. Lett.* **412**, 245–260.

Stichel T., Kretschmer S., Geibert W., Lambelet M., Plancherel Y., Rutgers Van Der Loeff M. and Van De Flierdt T. (2020) Particle–seawater interaction of neodymium in the North Atlantic. *ACS Earth Sp. Chem.* **4**, 1700–1717.

Stichel T., Pahnke K., Duggan B., Goldstein S. L., Hartman A. E., Paffrath R. and Scher H. D. (2018) TAG plume: Revisiting the hydrothermal neodymium contribution to seawater. *Front. Mar. Sci.* **5**, 96.

Stramma L. and England M. (1999) On the water masses and mean circulation of the South Atlantic Ocean. *J. Geophys. Res. Ocean.* **104**, 20863–20883.

Tachikawa K., Arsouze T., Bayon G., Bory A., Colin C., Dutay J. C., Frank N., Giraud X., Gourlan A. T., Jeandel C., Lacan F., Meynadier L., Montagna P., Piotrowski A. M., Plancherel Y., Pucéat E., Roy-Barman M. and Waelbroeck C. (2017) The large-scale evolution of neodymium isotopic composition in the global modern and Holocene ocean revealed from seawater and archive data. *Chem. Geol.* **457**, 131–148.

Tachikawa K., Jeandel C. and Roy-Barman M. (1999) A new approach to the Nd residence time in the ocean: The role of atmospheric inputs. *Earth Planet. Sci. Lett.* **170**, 433–446.

Tanaka T., Togashi S., Kamioka H., Amakawa H., Kagami H., Hamamoto T., Yuhara M., Orihashi Y., Yoneda S., Shimizu H., Kunimaru T., Takahashi K., Yanagi T., Nakano T., Fujimaki H., Shinjo R., Asahara Y., Tanimizu M. and Dragusanu C. (2000) JNdi-1: A neodymium isotopic reference in consistency with LaJolla neodymium. *Chem. Geol.* **168**, 279–281.

Taylor S. R. and McLennan S. M. (1985) *The continental crust: its composition and evolution*.

Tsuchiya M., Talley L. D. and McCartney M. S. (1994) Water-mass distributions in the western South Atlantic; a section from South Georgia Island (54S) northward across the equator. *J. Mar. Res.* **52**, 55–81.

Wilson D. J., Piotrowski A. M., Galy A. and Mccave I. N. (2012) A boundary exchange influence on deglacial neodymium isotope records from the deep western Indian Ocean. *Earth Planet. Sci. Lett.* **341–344**, 35–47.

Wyatt N. J., Milne A., Woodward E. M. S., Rees A. P., Browning T. J., Bouman H. A., Worsfold P. J. and Lohan M. C. (2014) Biogeochemical cycling of dissolved zinc along the GEOTRACES South Atlantic transect GA10 at 40°S. *Global Biogeochem. Cycles* **28**, 44–56.

Zheng X. Y., Plancherel Y., Saito M. A., Scott P. M. and Henderson G. M. (2016) Rare earth elements (REEs) in the tropical South Atlantic and quantitative deconvolution of their non-conservative behavior. *Geochim. Cosmochim. Acta* **177**, 217–237.

Zheng X., Yang J. and Henderson G. M. (2015) A robust procedure for high-precision determination of rare earth element concentrations in seawater. *Geostand. Geoanalyt. Res.* **39**, 277–292.

Zieringer M., Frank M., Stumpf R. and Hathorne E. C. (2019) The distribution of neodymium isotopes and concentrations in the eastern tropical North Atlantic. *Chem. Geol.* **511**, 265–278.

Associate editor: Tina van de Flierdt